Evaluation of the neutronic boundary conditions used in the diffusion analysis model of the PBMR core

Vishnu Visvanathan Naicker

Dissertation submitted in partial fulfillment
of the requirements for the degree
Magister in Science
School of Nuclear Engineering
at the
North-West University

Supervisor: Mr F. Reitsma
Centurion, 2006

ABSTRACT

The definition of boundary conditions are an important part of all core neutronics models. In the CITATION model, used as part of the VSOP core simulation, the neutronic boundary condition is defined in terms of an extrapolation constant called α. In this work, the definition of α, the sensitivity of the neutronic results to changes in α and the appropriate value of α for the PBMR 400MW core design is determined.

The value $\alpha = 0.4692$ used in the current model of VSOP has been shown to represent a vacuum boundary condition. Decreasing this value in the VSOP calculations to 0.3 does not change the reactivity significantly, but decreasing it further below that shows a significant increase in the calculated core reactivity.

The appropriate value of α was determined from a transport 1-D model using XSDRNPM calculations and yielded a value of $\alpha = 0.11414$. In this case, the core barrel and the reactor pressure vessel were included in the neutronic calculation, so that the influence of these structures which lie beyond the neutronic boundary in the VSOP analysis would be included.

The change in reactivity in the VSOP model when the default ($\alpha = 0.4692$ representing vacuum) and newly determined ($\alpha = 0.11414$) are used compares well with similar MCNP and XSDRNPM calculations where either a vacuum boundary condition or the actual geometry (barrel and reactor pressure vessel) was modelled. These values are 249 pcm (VSOP), 150 ± 40 pcm (MCNP) and 219 pcm (XSDRNPM) respectively.

In this work both a corrected extrapolation constant $\alpha = 0.11414$ and a methodology to calculate it from a reference 1-D transport solution was determined.

Declaration

I, the undersigned, hereby declare that the work contained in this project is my own original work.

Vishnu Visvanathan Naicker

Date: 6 December, 2006
Centurion

Dedication

In memory of my Aunt

Sheila Premavathi Govender

26/09/1937 – 7/11/2006

Acknowledgments

Mr F. Reitsma, under whom this work was done, for his expert guidance and professionalism

The VSOP team at Pebble Bed Modular Reactor (Pty) Ltd, for the many constructive discussions held regarding this work

Mrs Sandra van der Merwe, for editing this dissertation and still smiling afterwards

My friends, family and colleagues for their encouragement whilst I undertook this project

Pebble Bed Modular Reactor (Pty) Ltd, for the use of their facilities and sponsorship for the MSc. degree

My God in heaven, who is always a source of strength

Table of Contents

Abbreviations

Abbreviation or Acronym	Definition
AVR	Arbeitsgemeinschaft Versuchsreaktor (German for Jointly-operated Prototype Reactor)
CB	Core Barrel
EG	Energy Group
eq	equation
HTGR	High-temperature Gas-cooled Reactor
HTR	High-temperature Reactor
k_{eff}	Effective multiplication factor
MCNP	Monte Carlo N-particle Transport Code
MEDUL	MeherfachDUrchLauf (German for recirculation)
NNR	National Nuclear Regulator (RSA)
PBMR	Pebble Bed Modular Reactor
PBMR (Pty) Ltd	Pebble Bed Modular Reactor (Propriety) Limited
Pg	Page
RPV	Reactor Pressure Vessel
SAR	Safety Analysis Report
SiC	Silicon Carbide
THTR	Thorium High-temperature Reactor
TINTE	Time Dependent Neutronics and Temperatures
TRISO	Triple Coated Isotropic Particle
USA	United States of America
VSOP	Very Superior Old Program
VSOP99	VSOP (Very Superior Old Program) version 99
1-D	1 Dimensional
2-D	2 Dimensional

List of Figures

List of Tables

1. INTRODUCTION

1.1 Background

Currently, in South Africa, nuclear energy as a source of electric power generation comprises about 6.5% of the total electrical power produced [1]. This nuclear power is generated by two French-built pressurized water reactors located at Koeberg near Cape Town. Conventional UO_2 fuel rod assemblies are used as fuel. These assemblies are manufactured by Westinghouse Electric Company in the USA and Framatome-ANP in France. The Pebble Bed Modular Reactor (PBMR) will be a second type of reactor to be operating in South Africa at Koeberg, with the fuel being manufactured at Pelindaba in South Africa.

The PBMR is a High Temperature Gas Cooled Reactor (HTGR) that is currently being designed in South Africa by Pebble Bed Modular Reactor (Proprietary) Limited, hereafter referred to as PBMR (Pty) Ltd. It will have an expected capacity of 400 MW of thermal power. It is expected that commercial power production will commence in 2013.

There are many reasons for the development of the PBMR, and two of these are listed below.

- In order to advance nuclear energy to meet future energy needs, ten countries, including South Africa, formed the Generation IV forum (GIF). This forum proposed developing future generation nuclear systems that can be licensed, constructed, and operated in a manner that will provide competitively priced and reliable energy products while satisfactorily addressing nuclear safety, waste, proliferation, and public perception concerns. There are six such systems that have been selected for research and development. The PBMR falls within one of these designs, namely High Temperature Gas Cooled Reactors (HTGRs) [2].

- The reactor has inherent safety features because the reactor will not experience a core meltdown under accident conditions, and the design of the fuel elements reduces the emission of radioactive materials to levels below that which is allowable. Reference [3] gives detailed explanations of the HTR safety aspects.

The first reactor will be a demonstration plant, and once proven, will serve as the prototype for many more reactors to be built for the South African power utility ESKOM. The reactor is also being designed in modular form, where each module will produce 400 MW of thermal power. This means that for higher demands of power, packs of 6 or 8 modules will be coupled together to produce the required demand.

Other important consequences following the success of the PBMR would be that the reactors can be supplied to other countries in the developing world and that the reactors can also be an energy source for process heat applications. Reference [4] outlines the economic worth of the reactor and the inherent safety of the reactor.

In addition to PBMR (Pty) Ltd developing this type of reactor in South Africa, China started construction of a 10 MW High Temperature Reactor (HTR) in 1995. This reactor has been in full operation since 2002. Both the South African PBMR and the Chinese HTGR are based on the German HTGR technology.

The first HTGR in Germany, the AVR (Arbeitsgemeinschaft Versuchs Reaktor) [5], was a 46 MW thermal reactor, which was in operation from 1965 to 1988. The coolant in the core was helium, and the coolant loop was coupled to a steam cycle loop. In the latter years of operation the fuel loaded was TRISO coated UO_2 particles embedded in graphite spheres, using the MEDUL cycle.

The South African PBMR design uses graphite as a moderator and helium as the coolant. The fuel is made of low enriched uranium dioxide kernels of

0.5 mm diameter encased in layers of graphite and SiC, forming what is known as TRISO particles. These in turn are embedded in graphite and form the fuel zone of radius 2.5 cm. Encasing this fuel zone is a graphite shell of thickness 0.5 cm. The resulting fuel sphere comprising the fuel zone and the shell has a radius of 3.0 cm. The MEDUL fuel cycle is used (MEDUL is a German acronym meaning multiple recirculation), where the fuel spheres are cycled through the reactor six times on average. The thermodynamic cycle on which the system is based is the Brayton cycle. The turbo machinery consists of a turbine, compressor, and generator, with a gear box to regulate the speed of the generator. Other elements of the system are a recuperator, pre-cooler and the intercooler.

Some of the work that is currently being done by PBMR (Pty) Ltd involves designing the reactor for operation purposes and preparing the Safety Analysis Report (SAR) to be forwarded to the National Nuclear Regulator of South Africa (NNR). This SAR forms part of the application for the license to construct and operate the reactor. As described in the next section, the work in this dissertation forms part of the basis for the calculations in the SAR.

1.2 Motivation for this Work and Dissertation Objectives

The central aspects when modeling the core is to determine the neutron flux distribution in the core and the surrounding material, which includes the reflector regions. It is standard practice to define a boundary condition for any model of a physical entity. The boundary condition typically excludes areas of the problem not essential for the purpose of the study or model. This is needed not only to save time but also to ensure a solution in many applications. In VSOP [6],[7] and specifically in the CITATION finite difference solution, two boundary conditions must be defined in the radial direction when the system is modeled in cylindrical coordinates, one at the centre of the cylindrical system, and the other at the outer surface of the cylindrical system. Traditionally, the outer surface of the side reflector of the core was selected as the outer boundary of the problem.

The selection of the boundary condition to be at the reflector outer surface has a few motivating factors:

- Traditionally, HTR designs have a side reflector of at least 1 m thick that will render the boundary condition unimportant. This simplifies the problem in that a black boundary condition can be modeled which implies a non-reentrant neutron current.
- The void region between the side reflector and barrel cannot be easily modeled, so defining the boundary condition before the void region will circumvent this problem.
- The cross sections of the specific metallic composition might not be available in standard libraries and the scattering cross sections of the nuclides that constitute the barrel and Reactor Pressure Vessel (RPV) may then have to be updated.
- Diffusion theory might not be applicable so far from the core. At the barrel and RPV the flux is probably no longer isotropic, which could put diffusion solutions in doubt.

From these arguments it is clear that the selection of the outer reflector outer boundary is a natural choice of position for applying a boundary condition. This study will not try to justify the selection of this boundary any further, but rather it will focus on the appropriate boundary condition to be applied at this boundary for the current PBMR 400 MW VSOP model.

The boundary condition is defined by alpha (α) as

$$\alpha = -D\frac{d\phi/dx}{\phi}$$

where D is the diffusion constant and ϕ is the neutron flux. This α value is called the "external extrapolated boundary constant" [6].

In the current model of VSOP [8] the value for alpha at the edge of the side reflector is set at the default value 0.4692, recommended in the VSOP manual [6]. The first objective is to show that this value corresponds to a void region being present beyond the boundary.

However, defining a void boundary condition on the outer boundary of the side reflector is not optimal because there is material beyond the chosen boundary. The α corresponding to the specific neutron leakage including the presence of this material should therefore be calculated.

The second objective of this study is thus to establish a methodology on how to determine the α and to calculate it for the current model. It should be noted that this is the main objective of this study.

In this work, the value of alpha will be calculated using the computer code XSDRNPM [9]. However, the applicability of the XSDRNPM model to the VSOP model needs to be studied. This is a third objective of this study, and will also include sensitivity studies based on varying α.

The fourth objective of this study is to verify the diffusion model, when applying the determined alpha value, against the reference transport solution.

This study is important for the following reasons.
First, the value of α is expected to affect the reactivity and is thus important for core neutronic design, which includes estimating the initial core critical height. Second, the value of α will influence the flux and power profiles, the influence on control reactivity worths, the fluxes in the side reflector (which are important in evaluating the damage to graphite) and estimated fluences on metallic structures (although the estimation of ex-core fluences is only approximate in the diffusion approximation and a reference transport solution should rather be used). Third, the determination of α forms part of the outstanding issues registered against the current input model for the PBMR. Resolving these issues forms part of the work in completing the SAR. Finally, obtaining a more correct value for α will lead to greater confidence in the model.

1.3 Layout of Dissertation

The dissertation is presented in nine chapters, including this introduction chapter and the last chapter, which contains the appendices.

In chapter 2, a brief presentation on the theory of neutron transport is given. There is particular emphasis on diffusion theory, which is applicable in the VSOP code, and discrete ordinates solutions, which are applicable in the XSDRNPM code. The various equations regarding the constant α, as used in this work, are also presented.

Chapter 3 focuses on the methodology used. A short description of the VSOP and XSDRNPM codes is given, together with the geometrical layout of the reactor modelled in these codes. The method followed to calculate α is also presented. Further, the running of VSOP and XSDRNPM codes are discussed, together with the changes in input as required for this work.

Chapter 4 deals with the initial studies with XSDRNPM and VSOP. These studies include establishing whether an accurate value for α is necessary, and sensitivity studies regarding the models of XSDRNPM.

In chapter 5, the value for α is calculated using XSDRNPM. K_{eff} is then evaluated using the recommended α and the resulting change in reactivity with the alternate calculations of XSDRNPM and MCNP are compared.

In addition to determining α, other related aspects of the solutions of XSDRNPM and VSOP were studied and these are reported in chapter 6.

The conclusion of this work is presented in chapter 7. This includes recommendations on the boundary conditions that should be implemented in VSOP models. Further work that is possible is also presented.

Chapter 8 is the Bibliography.

The appendices are in chapter 9. Appendix A contains a sample input file for XSDRNPM, appendix B contains the listing of the ".fil" files, and appendix C is a listing of the program code used to extract data from the XSDRNPM output and to calculate the partial currents, and finally α.

1.4 Notation

The notation used are given in Table 1.

Table 1: Notation Used

D	Diffusion constant
k_{eff}	Effective multiplication factor
α	External extrapolated boundary constant
$\tilde{a}$	Extrapolation length
J_- J_+	Inward and outward partial currents, respectively
$\Sigma_t(\vec{r},E)$	Macroscopic cross section, in this instance it is the total macroscopic cross section for energy E
Δ	Mesh spacing
$\psi(\vec{r},E,\vec{\Omega})$	Angular Neutron Flux at position $\vec{r}$, with energy E and in direction $\vec{\Omega}$
ρ	Reactivity
λ_{tr}	Transport length

2. THEORY

For more detailed discussions on the theory, the reader is referred to [10], [11], [12].

2.1 The General Form of the Boltzmann Equation [9]

The time-independent Boltzmann transport equation that describes the neutron balance in a reactor can be written as

$$\vec{\Omega}\cdot\nabla\psi(\vec{r},E,\vec{\Omega})+\Sigma_t(\vec{r},E)\psi(\vec{r},E,\vec{\Omega})=S(\vec{r},E,\vec{\Omega}) \quad (1)$$

This expression states that the losses due to leakage and collisions must be equal to the source of neutrons, at some point in space $\vec{r}$ with energy E and direction $\vec{\Omega}$. In this expression, $\Sigma_t(\vec{r},E)$ is the total macroscopic cross section at energy E of the medium, which is typically assumed isotropic, and $\psi(\vec{r},E,\vec{\Omega})$ is the angular flux.

The source term, $S(\vec{r},E,\vec{\Omega})$ has three components:

a scattering source term $S^{s}(\vec{r},E,\vec{\Omega})$

a fission source term $F(\vec{r},E,\vec{\Omega})$ and

a fixed source term, $Q(\vec{r},E,\vec{\Omega})$.

The scattering source term is given by

$$S^{s}(\vec{r},E,\vec{\Omega})=\int_0^{4\pi}d\vec{\Omega}'\int_0^{\infty}dE'\Sigma_s(\vec{r},E'\rightarrow E,\vec{\Omega}'\rightarrow\vec{\Omega})\psi(\vec{r},E',\vec{\Omega}') \quad (2)$$

The fission source term can be written as

$$F(\vec{r},E,\vec{\Omega})=\frac{1}{4\pi k}\chi(\vec{r},E)\int_0^{4\pi}d\vec{\Omega}'\int_0^{\infty}dE'\nu(\vec{r},E')\Sigma_f(\vec{r},E')\psi(\vec{r},E',\vec{\Omega}'). \quad (3)$$

where

$\Sigma_s(\vec{r},E'\rightarrow E,\vec{\Omega}'\rightarrow\vec{\Omega})$ is the macroscopic double differential scattering cross section per unit energy for scattering from energy E' to E and direction $\vec{\Omega}'$ to $\vec{\Omega}$,

$\chi(\vec{r},E)$ is the fraction of the fission neutrons per unit energy produced at $\vec{r}$ and E,

$\nu(\vec{r},E)$ is the average number of neutrons produced per fission,

$\Sigma_f(r,E)$ is the macroscopic fission cross section and

k is the "effective multiplication factor."

2.2 Aspects of Diffusion Theory of Neutron Transport [13]

2.2.1 The Diffusion Equation

The transport equation, eq 1, can be written in the diffusion theory formalism if the following assumptions can be made about the system under consideration [12].

- The flux is assumed to be sufficiently slowly varying in space,

- absorption is small relative to scattering, and

- Fick's law holds in the following form:

$$\vec{J} = -D\nabla\phi \tag{4}$$

where D is the diffusion constant.

Then a basic equation expressing the diffusion approximation to neutron transport at some location $\vec{r}$ and energy E can be written as [13]

$$\begin{aligned} &-\nabla D(r,E)\nabla\phi(r,E)+(\Sigma_a(r,E)+\Sigma_s(r,E))\phi(r,E) \\ &=\int_{E'}dE'\left(\Sigma_r^{E'\to E}+\frac{\chi(E)\nu\Sigma_f(r,E')}{k}\right)\phi(r,E') \end{aligned} \tag{5}$$

Eq 5 can be simplified to eq 6 when the following is done:

- the continuous energy spectrum is divided into discrete energy groups

- a buckling term is allowed when appropriate

- the source distribution function $\chi(E)$ is assumed to have no spatial dependence

- a simplification is made in the transport term [13]

$$\begin{aligned} &-D_g(r)\nabla^2\phi_g(r)+\left(\Sigma_a^g(r)+\sum_n\Sigma_s^{g\to n}(r)+D_g(r)B_g^2\right)\phi_g(r) \\ &=\sum_n\left(\Sigma_s^{n\to g}(r)+\frac{\chi_g\nu\Sigma_f^n(r)}{k}\right)\phi_n(r) \end{aligned} \tag{6}$$

In this equation, ∇^2 is the Laplacian geometric operator,

$\phi_g(r)$ is the scalar neutron flux at location $\vec{r}$ and in energy group g,

$\Sigma_a^g(r)$ is the macroscopic cross section for absorption, normally weighted over a representative flux energy spectrum,

$\Sigma_s^{g\to n}(r)$ is the macroscopic cross section for scattering of neutrons from energy group g to energy group n,

$D_g(r)$ is the diffusion coefficient, normally one-third of the reciprocal of the transport cross section,

B_g^2 is the buckling term to account for the effect of the Laplacian operator (leakage) in a dimension not treated explicitly,

$\nu\Sigma_f^g(r)$ is the macroscopic production cross section, (ν) is the number of neutrons produced by a fission and Σ_f is the cross section for fission,

χ_g is the distribution function for source neutrons, and

k is the effective multiplication factor, ratio of rate of production of neutrons to rate of loss of neutrons from all causes, an unknown to be determined.

2.2.2 Finite Difference Solution of the Diffusion Equation

In order to solve eq 6, one approach is to solve the equation numerically using a standard finite difference formulation. Here, a mesh is established in the spatial geometry, where each point of the mesh is a point for the numerical analogue of eq 6. The Laplacian operator ∇^2 with respect to a given point is written in the usual manner in terms of the neighbours of the point. An iterative procedure incorporating energy group to group coupling is then carried out to determine the fluxes at the spatial mesh points for all the energy groups.

2.2.3 Boundary Conditions

To obtain a solution using the finite difference method, boundary conditions must be established at the boundaries of the system. Mathematically, this amounts to setting the number of equations available to be equal to the numbers of unknowns that must be solved. The boundary equations in this case are specified by the external extrapolated boundary constant α.

To establish the origin of the external extrapolation constant α, consider a mesh that lies on a given boundary, and for brevity, assume that this is an external boundary. Let ϕ_c be the internal flux in this mesh at some internal point, typically chosen to be the centre, ϕ_a to be the flux on the boundary, and Δ to be the distance from the internal point to the boundary.

Given the slope of the flux at the boundary, a point will exist at a distance $\tilde{a}$ from the boundary at which the flux can be extrapolated to zero, irrespective of whether void or material exists beyond the boundary.

From Figure 1 the slope m at the boundary can be written as

$$m = \frac{\phi(a+\tilde{a})-\phi(a)}{(a+\tilde{a})-a} = \frac{0-\phi(a)}{a+\tilde{a}-a} = -\frac{\phi(a)}{\tilde{a}} = -\frac{\phi_a}{\tilde{a}}$$

i.e.,

$$m = -\frac{\phi_a}{\tilde{a}} \tag{7}$$

Also, by definition of the gradient,

$$m = \left.\frac{d\phi}{dx}\right|_{x=a} \tag{8}$$

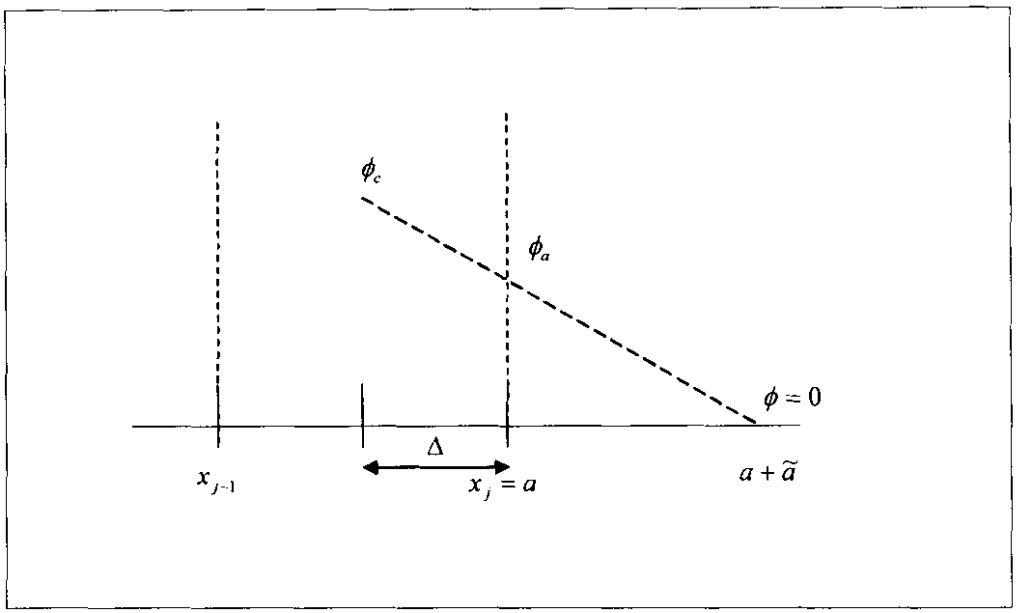

Figure 1: Representation of Flux at Problem Boundary in Finite Difference Approach

Equating 7 and 8 we get

$$-\frac{\phi_a}{\tilde{a}} = \left.\frac{d\phi}{dx}\right|_{x=a}$$

Rearranging this becomes

$$-\frac{d\phi/dx|_{x=a}}{\phi_a} = \frac{1}{\tilde{a}} \tag{9}$$

However, we can also write the gradient at boundary as

$$-\frac{\partial\phi}{\partial x} = \frac{\phi_c - \phi_a}{\Delta} \tag{10}$$

Thus, from eq 10 and 9 we get the boundary condition

$$\frac{\phi_c - \phi_a}{\Delta} = -\frac{\phi_a}{\tilde{a}} \tag{11}$$

which, when used in the finite difference formulation, is the equation needed to complete the system of equations.

The extrapolation length $\tilde{a}$ can be written in terms of the transport length λ_{tr} as

$$\tilde{a} = k_{mat}\lambda_{tr} \tag{12}$$

where k_{mat} is a parameter that depends on the material beyond the boundary point. Using the diffusion theory relation [12]

$$\lambda_{tr} = \frac{1}{\Sigma_{tr}} = 3D$$

eq 12 becomes

$$\tilde{a} = k_{mat}3D \tag{13}$$

where D is the diffusion constant. Eq 9 then becomes

$$-D\frac{d\phi/dx\big|_{x=a}}{\phi(a)} = \frac{1}{3k_{mat}} \tag{14}$$

We now define alpha as

$$\alpha = \frac{1}{3k_{mat}}$$

to get

$$-D\frac{d\phi/dx}{\phi} = \alpha \tag{15}$$

When the medium beyond the boundary is a void, then it is shown in [14] that $k_{mat} = 0.7104$. This is the solution to the "Milne Problem" which determines the neutron distribution everywhere in an infinite source-free half space with zero incident flux.

Substituting this value for k_{mat} into eq 14, we then get

$$-D\frac{d\phi/dx}{\phi} = 0.4692 \tag{16}$$

which is the result that is used in VSOP [6]. With this derivation, the first objective of this study is fulfilled.

Further from eq 9 and eq 15 we get that

$$\frac{\alpha}{D} = \frac{1}{\tilde{a}} \tag{17}$$

Considering Figure 1, we note that the extrapolation length for a given geometry will increase from that due to the void when a scattering material is present beyond the boundary. If a strong absorber is present beyond the boundary, this extrapolation length will decrease from that due to the void. This means that for the present study, from eq 17, the maximum value that α can have is 0.4692.

2.3 Aspects of Discrete Ordinates solution to the Transport Equation

The following theory is explained in detail in [9] and is included here since the XSDRNPM code is based on this formalism.

2.3.1 Multigroup One-Dimensional Boltzman Equation

In multigroup schemes, the point-energy balance equation, eq 1, is converted to multigroup form similar to that of the diffusion formulation, by first selecting a suitable energy structure. The multigroup equivalent of the point equation is then written according to this structure which requires multigroup constants that tend to preserve the reaction rates that would arise from integrating the point equations by group. If we designate the groups by g, so that

$$\psi_g(x,\mu) = \int_g dE\,\psi(x,E,\mu)$$

and

$$\psi_g(x) = \int_{-1}^{1} d\mu\,\psi_g(x,\mu)$$

then the following form of the 1-D Boltzmann equation can be derived for the slab geometry:

$$\mu \frac{\partial \psi_g(x,\mu)}{\partial x} + \Sigma_t^g(x)\psi_g(x,\mu) = S_g(x,\mu) + F_g(x,\mu) + Q_g(x,\mu) \tag{18}$$

The equations for the cylinder and sphere are essentially the same except for the differences in the leakage terms.

In eq 18, S_g, F_g and Q_g are the scattering, fission and fixed sources, respectively.

2.3.2 The Fission Source Term

The multigroup form of the fission source of eq 18 is

$$F_g(x,\mu) = \frac{\chi_g}{2\pi k} \sum_{g'} \overline{\nu\Sigma_{fg'}}(x)\psi_{g'}(x,\mu)$$

where χ_g is the fraction of the fission neutrons that are produced in group g, $\overline{\nu\Sigma_{fg'}}$ is the average of the product of ν (the average number of neutrons produced per fission) and Σ_f (the fission cross section).

2.3.3 Scattering Source Term

In discrete ordinates theory, the Legendre moments of the flux, $\psi_{g,l}$ are typically defined by

$$\psi_{g,l} = \frac{1}{2}\int_{-1}^{1} d\mu \psi_g(\mu) P_l(\mu)$$

The group-to-group scattering coefficients are fit with Legendre polynomials, so that

$$\sigma(g' \to g, \mu) = \sum_{l=0}^{L} \frac{2l+1}{2} \sigma_l(g' \to g) P_l(\mu) \tag{19}$$

In this equation, we have a fit of order *L*.

2.3.3.1 Slab and Spherical Geometries

Because of the symmetries in 1-D slabs and spheres, only one angle is needed to describe a "direction." In the case of the slab, the angle is taken with reference to the x-axis, while for the sphere, it is with reference to a

radius vector between the point and the centre of the sphere. This means that the flux can be expanded in ordinary Legendre polynomials, so that

$$\psi(r,E,\mu)=\sum_{l=0}^{\infty}\psi_l(r,E)P_l(\mu) \tag{20}$$

$$\psi(r,E)=\int_{-1}^{1}\frac{d\mu}{2}P_l(\mu)\psi_l(r,E,\mu) \tag{21}$$

When eq 20 and eq 21 are introduced into eq 2, the following expression is derived for the scattering source:

$$S(r,E,\mu)=2\pi P_l(\mu)\int_0^{\infty}dE'\int_{-1}^{1}d\mu'\sum_{l=0}^{L}\frac{2l+1}{1}\Sigma_{s_l}(r,E'\rightarrow E)P_l(\mu')\psi_l(r,E')$$

where L is the order of fit to the fluxes and cross sections.

2.3.3.2 Cylindrical Geometry

The situation is more complicated in the case of the 1-D cylinder where the flux (and cross section) must be given as a function of two angles.
In this case, the scattering source terms become

$$S(r,E,\mu)=\sum_{l=0}^{L}\frac{2l+1}{2}\int_0^{2\pi}dE'\sigma_{s_l}(\vec{r},E'\rightarrow E)$$
$$\times\left[P_l(\mu)\psi(\vec{r},E')+\sum_{n=1}^{l}\sqrt{2\frac{(l-n)!}{(l+n)!}}P_n^l(\mu)\cos n\zeta\psi_l^n(\vec{r},E)\right] \tag{22}$$

2.3.4 Discrete Ordinates Difference Equations

The Sn method is a discrete ordinates method that can be employed to solve the transport eq 1. In most cases however, more simplified forms of this equation are solved, e.g., that of eq 18 for the slab case.

In formulating the *Sn* equations, several symbols are defined which relate to a flux in an energy group g, in a spatial interval i, and in an angle m. Typically, the flux is quoted as an integral of the flux in an energy group g, the upper and lower bounds of which are E_g^U and E_g^L respectively.

$$\psi_g=\int_{E_g^L}^{E_g^U}dE\psi(E)$$

A mechanical quadrature is taken in space, typically IM intervals with IM + 1 boundaries. Likewise, an angular quadrature is picked to be compatible with the particular 1-D geometry, typically MM angles with associated directional coordinates and integration weights.

The different equations are formulated in a manner which involves calculating so-called angular fluxes, $\psi_{g,i,m}$ at each of the spatial interval boundaries, and also cell-centered fluxes $\psi_{g,i+\frac{1}{2},m}$ at the centers of the spatial intervals. The centered fluxes are related to the angular boundary fluxes by "weighted diamond difference" assumptions. In both cases the fluxes are integrated in energy over the group g.

2.3.4.1 Discrete Ordinates Equation for a Slab

Consider a spatial cell bounded by x_i, x_{i+1} and the loss term for flow through the cell in direction μ_m. The net flow in the x-direction out of the right side is the product of the angular flux times the area times the solid angle times the cosine of the angle:

$$w_m \mu_m A_{i+1} \psi_{g,i+1,m}$$

The net loss from the cell is the difference between the flows over both boundaries:

$$w_m \mu_m \left(A_{i+1} \psi_{g,i+1,m} - A_i \psi_{g,i,m} \right) \tag{23}$$

The loss in the spatial cell due to collisions is given by the product of the centred angular flux (in per unit volume units) times the total macroscopic cross section times the solid angle times the volume:

$$w_m \sigma_{g,i+\frac{1}{2}} V_i \psi_{g,i+\frac{1}{2},m} \tag{24}$$

The sources in direction μ_m are given by the product of the solid angle times the interval volume times the volume-averaged source (sum of fixed, fission, and scattering) in the direction m:

$$w_m V_i S_{g,i+\frac{1}{2},m} \tag{25}$$

The slab equation is obtained by using eq 23, eq 24, and eq 25 and substituting proper values for area and volume:

$$w_m \mu_m \left(\psi_{g,i+1,m} - \psi_{g,i,m}\right) + w_m \sigma_{g,i+\frac{1}{2}} \psi_{g,i+\frac{1}{2},m} \left(x_{i+1} - x_i\right) = w_m S_{g,i+\frac{1}{2},m} \left(x_{i+1} - x_i\right) \quad (26)$$

In an MM angle quadrature set, there are MM of these equations and they are coupled through the assumption of how the cell-centered flux relates to the boundary angular fluxes, the sources, and the boundary conditions.

2.3.4.2 Discrete-Ordinates Equations for Sphere and Cylinder

The development of the equations for these geometries is analogous to that for the slab except that the leakage terms are more complicated. For a sphere, consider Figure 2 in which a particle travels from point i to i+1, At i, the position and direction is r_i and μ_m respectively, and at i + 1, the position and direction is r_{i+1} and μ_m^*, The directions μ_m and μ_m^* are not the same. The same effect also exists for the cylinder, though in this case the direction coordinates are more complicated.

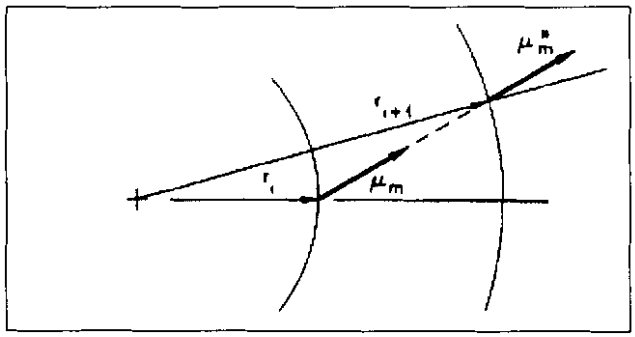

Figure 2: Angular Redistribution in Spherical Geometry [9]

Because of this effect, a loss term is included for the "angular redistribution." It is defined in a manner analogous to eq 23 as

$$\alpha_{i+\frac{1}{2},m+\frac{1}{2}} \psi_{g,i+\frac{1}{2},m+\frac{1}{2}} - \alpha_{i+\frac{1}{2},m-\frac{1}{2}} \psi_{g,i+\frac{1}{2},m-\frac{1}{2}} \quad (27)$$

where the α coefficients are to be defined in such a manner as to preserve particle balance. (This is not the external extrapolated boundary constant α). Obviously, it is necessary that the net effect of all redistributing be zero, in order to maintain particle balance. This condition is met if

$$\sum_{m=1}^{MM} \alpha_{m-\frac{1}{2}} \psi_{m-\frac{1}{2}} + \alpha_{m+\frac{1}{2}} \psi_{m+\frac{1}{2}} = \alpha_{\frac{1}{2}} \psi_{\frac{1}{2}} + \alpha_{MM+\frac{1}{2}} \psi_{MM+\frac{1}{2}} = 0 \quad (28)$$

where we have dropped the group and interval indexes.

In order to develop an expression for determining the $\alpha's$, consider an infinite medium with a constant isotropic flux. In this case, there is no leakage and the transport equation reduces to

$$\Sigma_t \phi = S \tag{29}$$

This condition requires that

$$\mu_m w_m \left(A_{i+1}\psi_{g,i+1,m} - A_i \psi_{g,i,m}\right) + \alpha_{i+\frac{1}{2},m+\frac{1}{2}}\psi_{g,i+\frac{1}{2},m+\frac{1}{2}} - \alpha_{i+\frac{1}{2},m-\frac{1}{2}}\psi_{g,i+\frac{1}{2},m-\frac{1}{2}} \tag{30}$$

which, when we note that all the ψ terms in the infinite medium case are equal becomes

$$\mu_m w_m \left(A_{i+1} - A_i\right) = -\alpha_{m+\frac{1}{2}} + \alpha_{m-\frac{1}{2}} \tag{31}$$

which is a recursion relationship for α. From eq 28 we see that the conservation requirement can be met if

$$\alpha_{\frac{1}{2}} = \alpha_{MM+\frac{1}{2}} = 0 \tag{32}$$

for any values of flux, and is, therefore, used to evaluate the $\alpha's$ along with eq 30 or eq 31.

The final discrete-ordinates expression for spheres and cylinders is then derived by summing expressions 23, 27 and 24 and setting it equal to expression 25.

2.3.5 Sn Quadratures for Cylinders

Since the slab and spherical geometries are not used in this project, it will not be discussed here.

The quadrature sets for cylinders are specifed by the directions defined with the two angles, ζ and η, where $\alpha = \sin\eta\cos\zeta$ and $\beta = \cos\eta$ β. See Figure 3, where $\zeta \equiv \xi$.

In this case, the practice is to use n/2 levels of directions for an n*th* order set. The levels correspond to fixed values of η. The number of angles by level starts with three in level 1, five in level 2, seven in level 3, etc. (Note that since cylindrical geometry is curvilinear, each level will start with a $\zeta = \pi$ direction

that has zero weight. Figure 4 shows the ordering of the directions for an S_6 quadrature set. Angles 1, 4, and 9 are the starting directions (zero weight) for the levels.

In general, an n*th* order quadrature will contain $n(n+1)/4$ angles.

These cylindrical quadrature sets are based on Gauss-Tschebyscheff schemes with Gaussian quadratures in β and Tschebyscheff quadratures in α. In this scheme, only the cosine μ is required in the formulation [9].

These cosines, μ and the weights are stored in two arrays internally in the code; and, since the weights for the 1^{st}, 4^{th}, and 9^{th} angles are zero, the cosines for the corresponding levels are placed in these locations in the arrays.

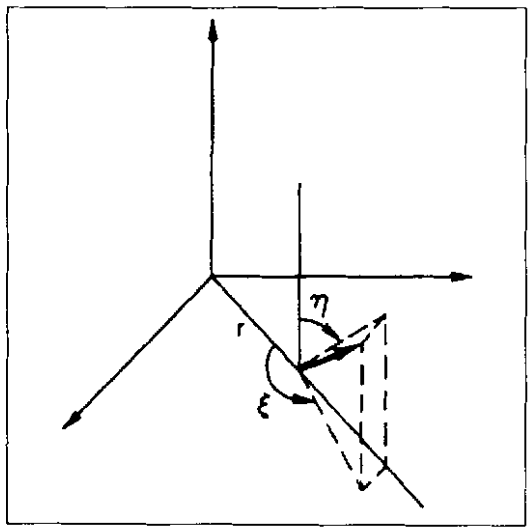

Figure 3: 1-D Cylindrical Coordinate System [9]

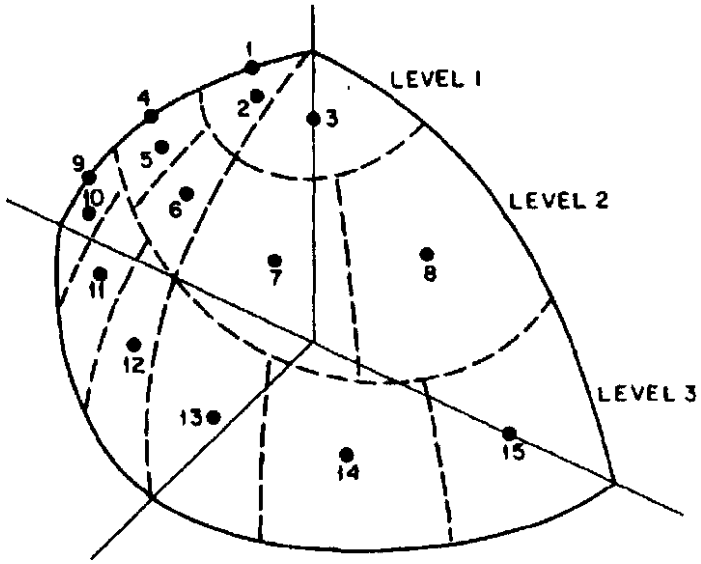

Figure 4: Ordering of the Directions for an S_6 Cylindrical Set [9]

2.3.6 Boundary Conditions

Boundary conditions can be specified in many ways. Some of the options most often used are the following:

1. Vacuum boundary — all angular fluxes that are directed inward at the boundary are set to zero (e.g., at the left-hand boundary of slab, $\psi(\mu > 0) = 0$, etc.).

2. Reflected boundary — the incoming angular flux at a boundary is set equal to the outgoing angular flux in the reflected direction (e.g., at the left-hand boundary of a slab),

$$\psi_{in}(\mu) = \psi_{out}(-\mu)$$

3. Periodic boundary — the incoming angular flux at a boundary is set equal to the outgoing angular flux in the same angle at the opposite boundary.

4. White boundary — the angular fluxes of all incoming angles on a boundary are set equal to a constant value so that the net flow across the boundary is zero, that is,

$$\psi_{in} = \frac{\sum_{m}^{out} w_m \mu_m \psi_m}{\sum_{m}^{in} w_m |\mu_m|}$$

This boundary condition is generally used as an outer-boundary condition for cell calculation of cylinders and spheres that occur in lattice geometries.

5. Albedo boundary — this option is for the white boundary condition except that a user-supplied group-dependent albedo multiplies the incoming angular fluxes.

2.3.7 Evaluation of Partial Currents using the Discrete Ordinate Method

At any given spatial position, the partial currents can be calculated using the equations

$$J_+ = \sum_{m=1}^{24} \psi_m \mu_m w_m \ , \ \mu_m > 0 \tag{33}$$

$$J_- = \sum_{m=1}^{24} \psi_m |\mu_m| w_m \ , \ \mu_m < 0 \tag{34}$$

where μ_m and w_m are the quadrature cosines and weights respectively, and ψ_m are the angular fluxes at each quadrature.

2.4 Evaluation of α from the Partial Currents J_- and J_+

The aim of this study is to calculate α from a transport solution. It is important first to establish the sign convention for the partial currents. Therefore, following [10], we define J_- as the inward current, and J_+ as the outward current.

Then, from [12], we get

$$J_- = \tfrac{1}{4}\Phi + \tfrac{1}{2} D \frac{\partial \Phi}{\partial x}$$

and

$$J_+ = \tfrac{1}{4}\Phi - \tfrac{1}{2} D \frac{\partial \Phi}{\partial x}$$

Dividing J_- by J_+ we get

$$\frac{J_-}{J_+} = \frac{\frac{1}{4}\Phi + \frac{1}{2}D\frac{\partial\Phi}{\partial x}}{\frac{1}{4}\Phi - \frac{1}{2}D\frac{\partial\Phi}{\partial x}} = \frac{\Phi + 2D\frac{\partial\Phi}{\partial x}}{\Phi - 2D\frac{\partial\Phi}{\partial x}}$$

Dividing by the flux, we then get

$$\frac{J_-}{J_+} = \frac{1 + 2D\frac{\partial\Phi}{\partial x}\Big/\Phi}{1 - 2D\frac{\partial\Phi}{\partial x}\Big/\Phi} \tag{35}$$

We now use the definition of α according to eq 15 and substitute for α. Eq 35 then becomes

$$\frac{J_-}{J_+} = \frac{1-2\alpha}{1+2\alpha} \tag{36}$$

Rearranging this equation, we finally get

$$\alpha = 0.5 \times \frac{1-C}{1+C} \tag{37}$$

where

$$C = \frac{J_-}{J_+}$$

2.5 The Monte Carlo Method for Determining k_{eff}.

The k_{eff} results from an MCNP (Monte Carlo n-particle transport code) calculation is used for comparison with the k_{eff} values obtained using VSOP and XSDRNPM. It is therefore felt necessary to present a short description of the theory underlying this method, which is stochastic, and the reader is referred to [15] for more detail.

The typical history of a neutron from birth to termination would involve the following events

- birth
- uncollided motion through the system

- scattering collisions
- absorption
- fission
- leakage out of the system

In a Monte Carlo code, each of these events is modeled stochastically using appropriate probability distributions for the sampling unless these events are governed by physical laws. (An example of a physical law is the conservation of linear momentum in scattering events). Termination of the history would normally occur when the neutron is absorbed, or it causes fission, or it leaks out of the system.

A given generation of neutrons is then specified by selecting a finite number, say N, of successive particle histories. The number of neutrons that arise from fission of this generation is calculated and yields the neutron population for the next generation.

The following generation is then simulated in a similar way, with the exception that the neutron source distribution is now specified by the distribution in space of the fission neutrons, which were born in the previous generation.

The k_{eff} is then calculated as the ratio of the neutron populations of two successive generations, $k_{eff} = \frac{N_{i+1}}{N_i}$.

3. CALCULATIONAL METHODOLOGY

3.1 Introduction

Much of the effort in designing the reactor is in developing computer models for the reactor operation. In particular, the neutronics and thermal hydraulics of the core are modelled using VSOP for steady state calculations [16], and TINTE for the transient states[7], [17].

In this chapter, a short description of the codes used in this study, viz. VSOP and XSDRNPM, are given, together with the geometrical layout of the reactor as modelled in these codes. Further, the running of VSOP and XSDRNPM codes are discussed, together with the changes in input as required for this work. The reader is referred to [7], [18] for further information on TINTE.

The method followed to calculate α is also presented.

3.2 Computer Codes used

The two codes used in this project were VSOP99 3_update2_July04 [19] which will be referred to as VSOP in this study, and XSDRNPM which is a part of SCALE 4.4 [20].

3.2.1 VSOP

VSOP (Very Superior Old Programs) is a code that was originally developed in Germany to model the neutronics and thermal hydraulics of high temperature reactors, e.g., the AVR, HTR-Modul and the THTR. It is now also used by the Chinese to model the HTR-10 [21].

VSOP is a system of proven computer codes linked together for the numerical simulation of the nuclear reactor. The calculation comprises the processing of the cross sections, reactor and fuel element design, neutron spectrum evaluation, 2 or 3 dimensional diffusion calculation, burnup, fuel shuffling,

control and, for the pebble bed HTR, thermal hydraulics of steady state and transients. Figure 5 shows the VSOP physics simulation.

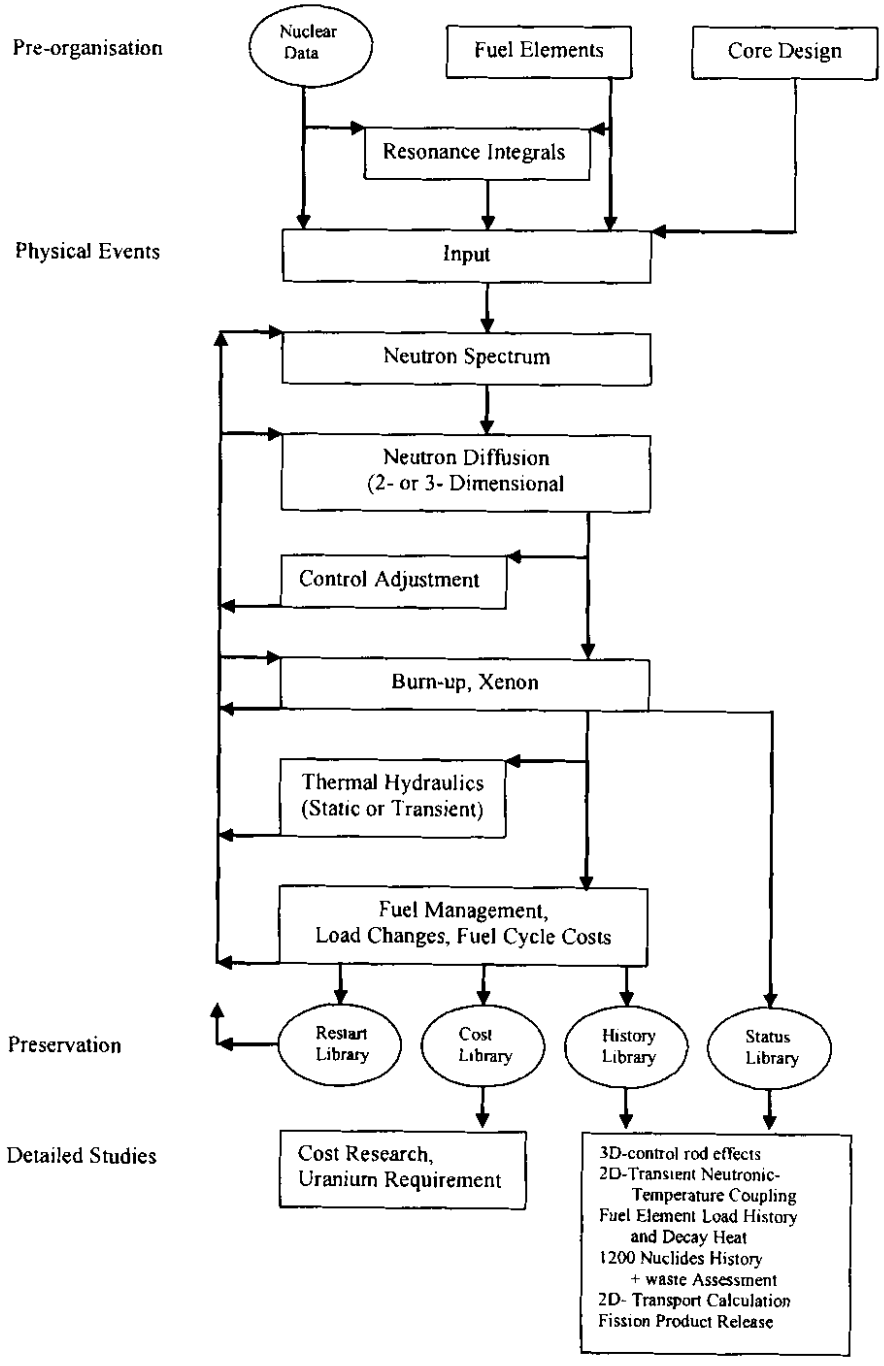

Figure 5: VSOP Physics Simulation [19]

Figure 6 shows the basic libraries and codes of which VSOP is made up.

- The two libraries GAM-I and THERMOS have been derived from the evaluated nuclear data files ENDF/B-V and JEF-1. The GAM-I library data is given in a 68 energy group structure ranging from 10 MeV through 0.414 eV. The THERMOS library data are given in 30 energy groups ranging from 10^{-5} eV through 2.05 eV.
- DATA-2 prepares the fuel element input data from its geometric design.
- BIRGIT prepares the 2-D geometric design of the reactor.
- Spectrum calculations are made by GAM-I and THERMOS for an unlimited number of spectrum zones.
- Diffusion calculations are made by the CITATION, which involves the solution of the diffusion equation.
- The burnup and the fuel shuffling is covered by FEVER for a number of burnup batches.
- THERMIX is included for the thermal hydraulics evaluation.

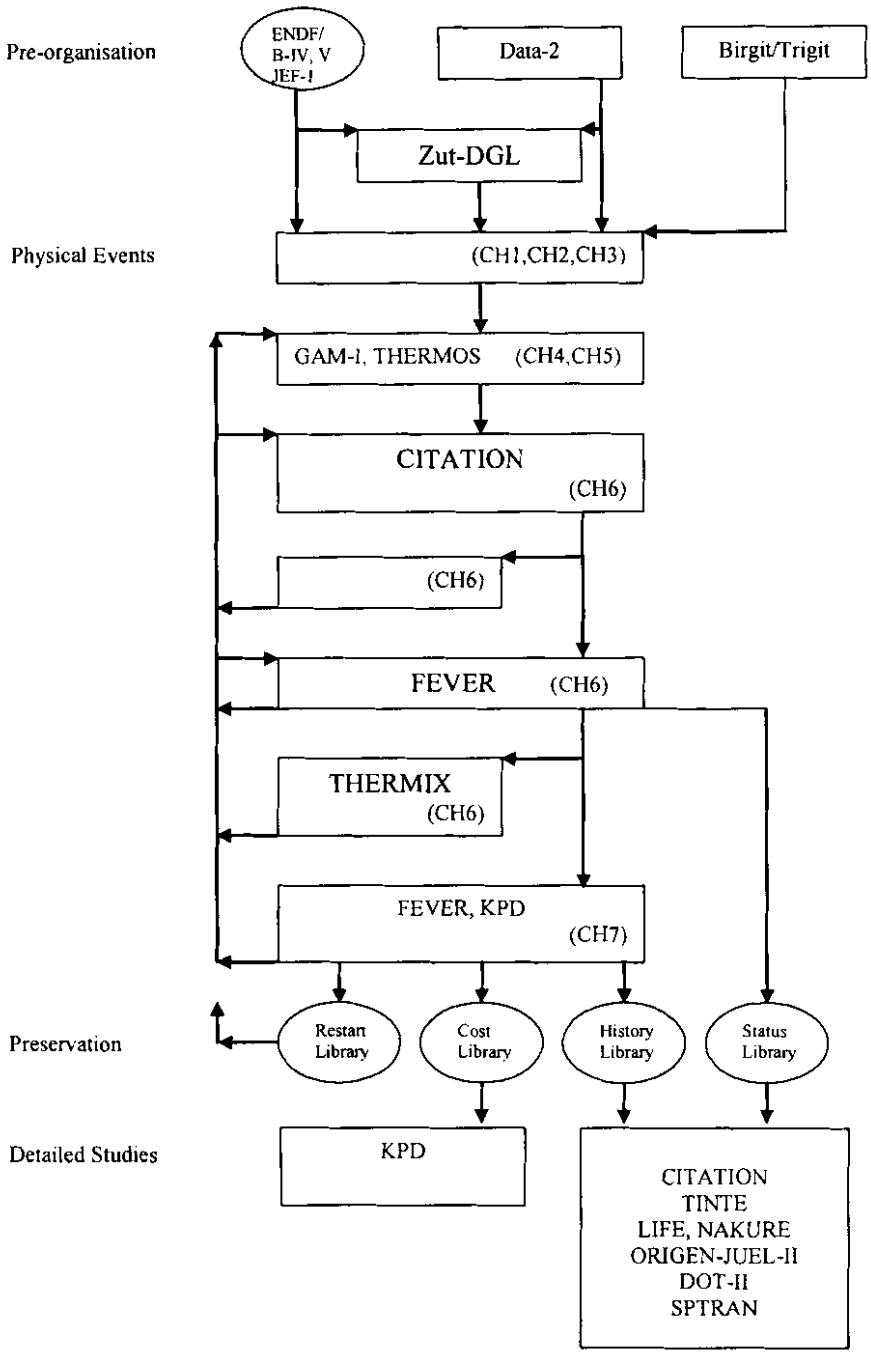

Figure 6: VSOP - The Basic Programs [19]

3.2.2 XSDRNPM

XSDRNPM is a one dimensional (1-D) discrete ordinates transport code and is part of the SCALE 4.4 suite of programs [20]. 1-D diffusion theory or infinite medium B_n calculations can also be made, as an option. In addition to this, XSDRNPM can also use the fluxes determined from its spectral calculation to collapse input cross sections and write these into one of several possible formats.

A flux calculation can be performed according to several options, including fixed source calculations, k_{eff}-calculations, and dimension search calculations. In this study it was used to perform 1-D discrete ordinates calculations in cylindrical geometry, in which k_{eff} was calculated.

The major program flow path of XSDRNPM is shown in Figure 7.

MAIN Program (named XSDRN) – calls SETUP to read the first data block and indirectly calls XSDRIV through ALOCAT. ALOCAT assigns core to XSDRIV which controls the rest of the run
SETUP Assigns some default values, opens several IO buffers and reads the first block of data
XSDRIV calls several subroutines which control major processes.
DRTRAN – reads the second data block, calls MIX to mix macroscopic data, calls PLSNT to read remaining data blocks, assigns other array space, and determines many constants needed elsewhere in the calculations.
OUTERS – control module for all flux calculations
OUTPUT – controls the editing of fine- and broad-group fluxes by interval
BT – controls balance table calculations
ACTY - controls activity table calculation
FEWG – controls cross-section weighting
SPOUT – controls production of ANISN and CCCC libraries

Figure 7: Main Program Flow of XSDRNPM [9]

Here, the routine "OUTERS" is the control module for all flux calculations, and the flow of this routine "OUTERS" is shown in Figure 8. In this routine, the routine "INNER" is called. "INNER" is the routine that does the discrete ordinates flux calculation. It uses the current scalar flux and flux moments to calculate the scattering source for the current group. It then loops over the angles, calculating the angular flux at each mesh boundary using a weighted diamond-difference scheme, traversing the mesh in the direction of the current angle. During the sweep, it computes an updated scalar flux and flux moments. When it reaches a system boundary, it saves the new boundary flux. A new eigenvalue on k_{eff} is calculated from the neutron balance and the iterations are continued until the required convergence criteria are met.

GEOMF -	Calculates areas, volumes, and other geometric parameters used in the flux calculation
FIXSRC -	Determines the integrals of the fixed sources by interval
WOT8 -	Called to edit geometrical parameters determined in GEOMF and FIXSRC
FISSRC -	Calculates the fission sources by interval from current flux values
SCATSC -	Calculates the inscattering sources (all moments) from current flux values
BN -	Called if a B_n calculation has been requested
CELL -	Called if an infinite medium calculation has been requested
DT/BDYFLX -	Called if a diffusion theory calculation has been requested.
INNER -	Called if a discrete ordinates calculation is requested
REBALN -	Called to do inner iteration scaling for discrete-ordinates
XCEL -	Writes binary-flux moments tape, if requested
SCALFC -	Generates the upscatter scaling factors
FXCEL -	Outer iteration flux acceleration is done here
CONVRG -	Called to check outer iteration convergence

Figure 8: OUTERS Calling Chart of XSDRNPM [9]

3.3 Geometry

The PBMR reactor is tall and narrow. Figure 9 shows a side view of the core structures, with the reactor pressure vessel as the outer structure. The reactor core is annular, and the core geometrical specifications are listed in Table 2.

This core is modeled using the computer code VSOP [6], where, for the neutronic calculations, the radial boundary is set at the outer side reflector edge. Figure 10 shows a schematic diagram of the reactor layout in which this boundary can be identified.

Table 2: Core Geometrical Specifications [22]

Description	Unit	Value
Core outer diameter	m	3.7
Core inner diameter	m	2.0
Effective cylindrical height of the core	m	11.0
Total volume of fuel zone	m^3	83.7156
Inner diameter of the core barrel	m	5.750
Wall thickness of the core barrel	m	0.06
Inner diameter of the Reactor Pressure Vessel (RPV)	m	6.2
Wall thickness of the RPV	m	0.180

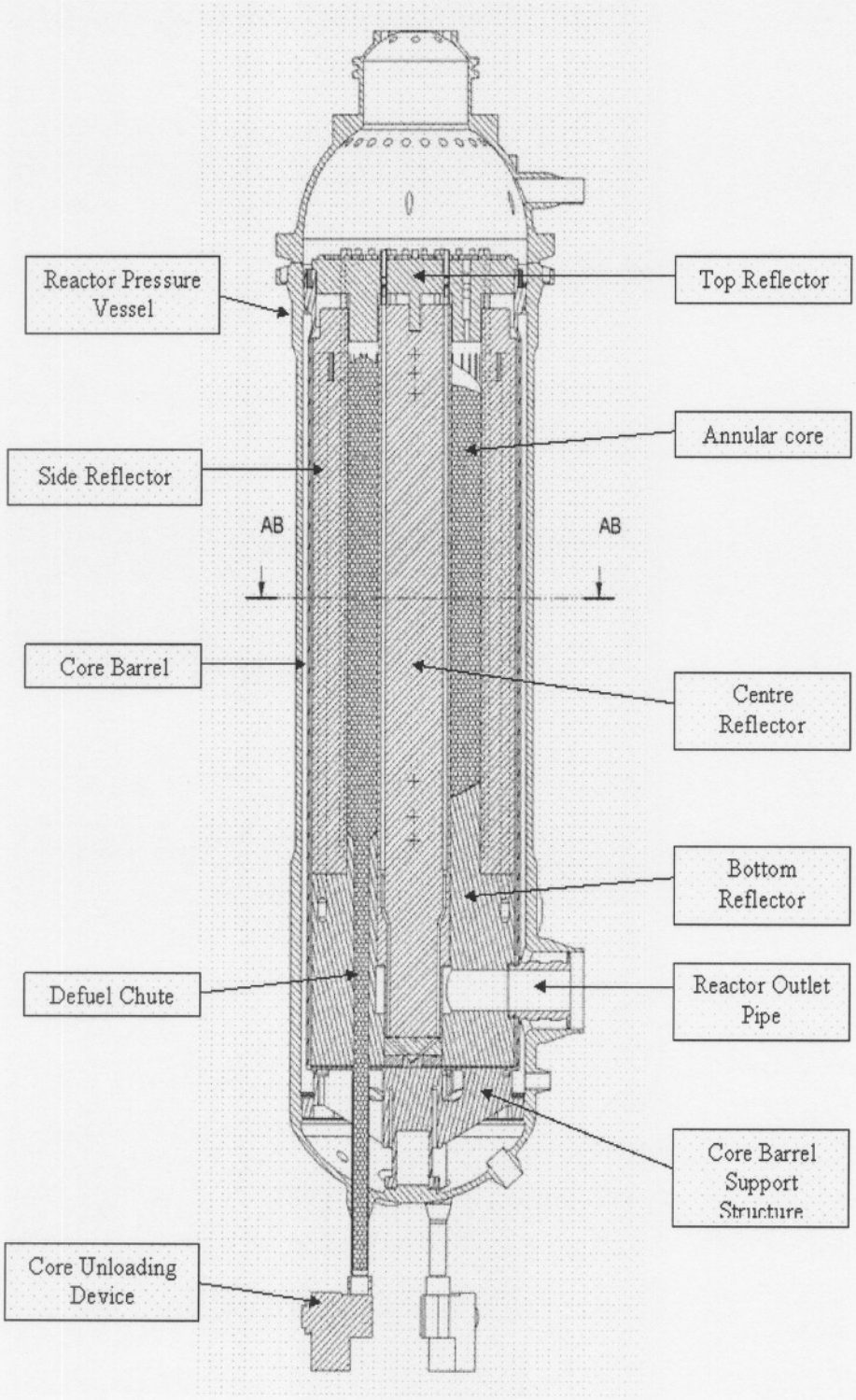

Figure 9: Core Layout Side View [22]

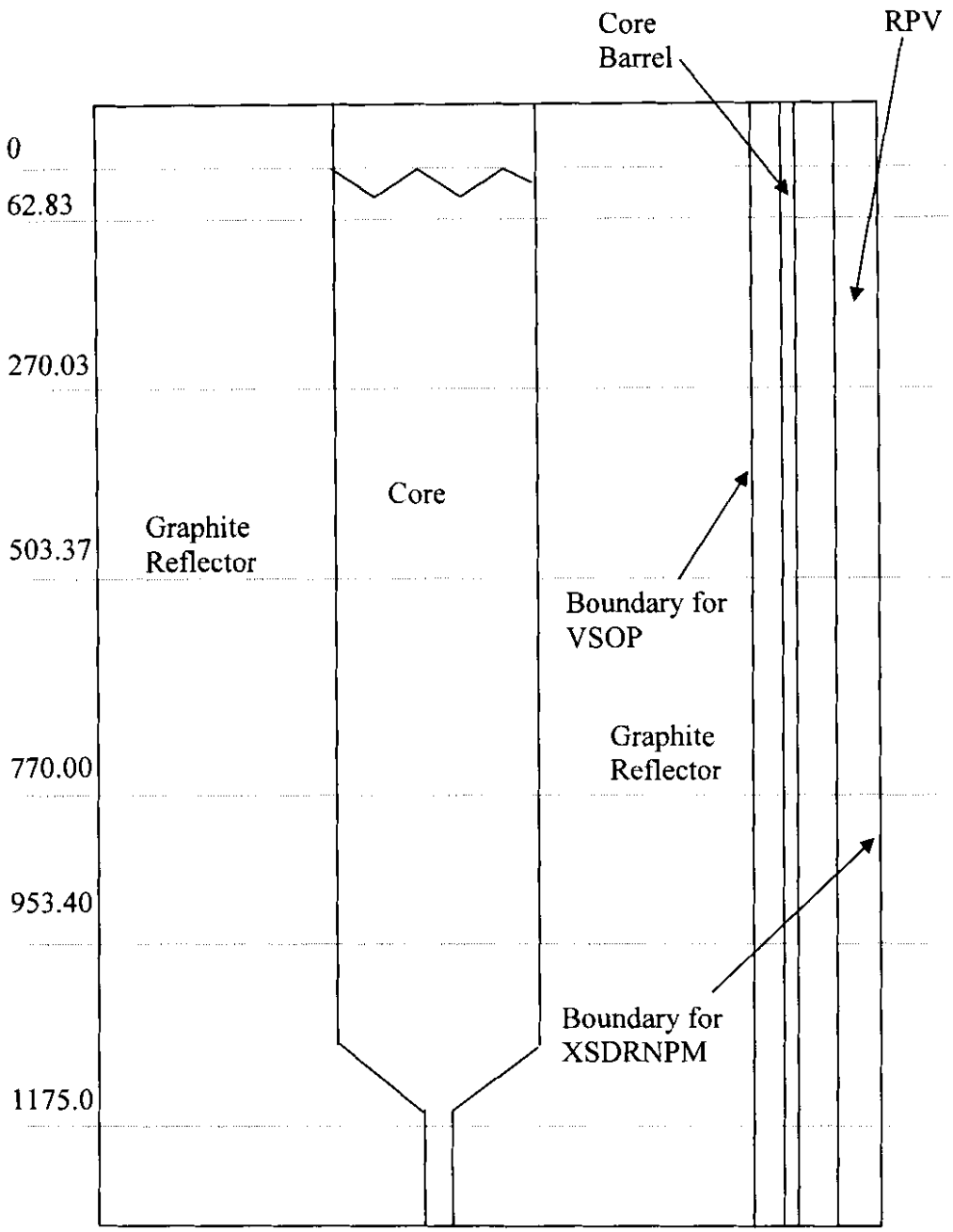

Figure 10: Schematic of the Reactor Layoutt

3.3.1 Geometrical Layout of VSOP

Once the components of the reactor core and surrounding structures are selected as part of the analysis domain, these components must then be modeled geometrically in a suitable manner in a 2-D VSOP model. This is done by defining material regions for the various components, and is shown in Figure 11. Note that the dotted lines above region 46, to the right of region 169 and below region 56, define the neutronic boundaries for the CITATION calculations. The material specification for each region is listed in Table 3.

3.3.2 Geometrical Layout in XSDRNPM

To model the geometry in 1-D for XSDRNPM, the reactor core and part of the surrounding structures were also selected as the analysis domain. In the available XSDRNPM model [26] (called the reference case), this domain was broken up into zones as is shown in Figure 12B. The materials specified in each zone are also indicated in the figure. Each zone was subdivided into meshes for the numerical calculations performed by XSDRNPM.

In the present study, where the focus is on the neutronic behaviour at the outer boundary of the reactor, the requirement was to represent the core barrel (CB) and the reactor pressure vessel (RPV) explicitly and not homogenized as in the available model. Therefore, zone 10 of Figure 12 B, where a homogeneous representation of the CB and the RPV was used was separated into zones 10, 11, 12, 13, i.e., a more correct heterogeneous representation. The material in each of these zones is helium, CB, helium and RPV respectively. For comparison, the material specification according to a simulated 1-D representation of VSOP model is shown in Figure 12A. A reflective boundary condition was set at the centre of the reactor (inside edge of zone 1), and a void boundary condition was set on the outer surface of the reactor (at the outer edge of zone 13).

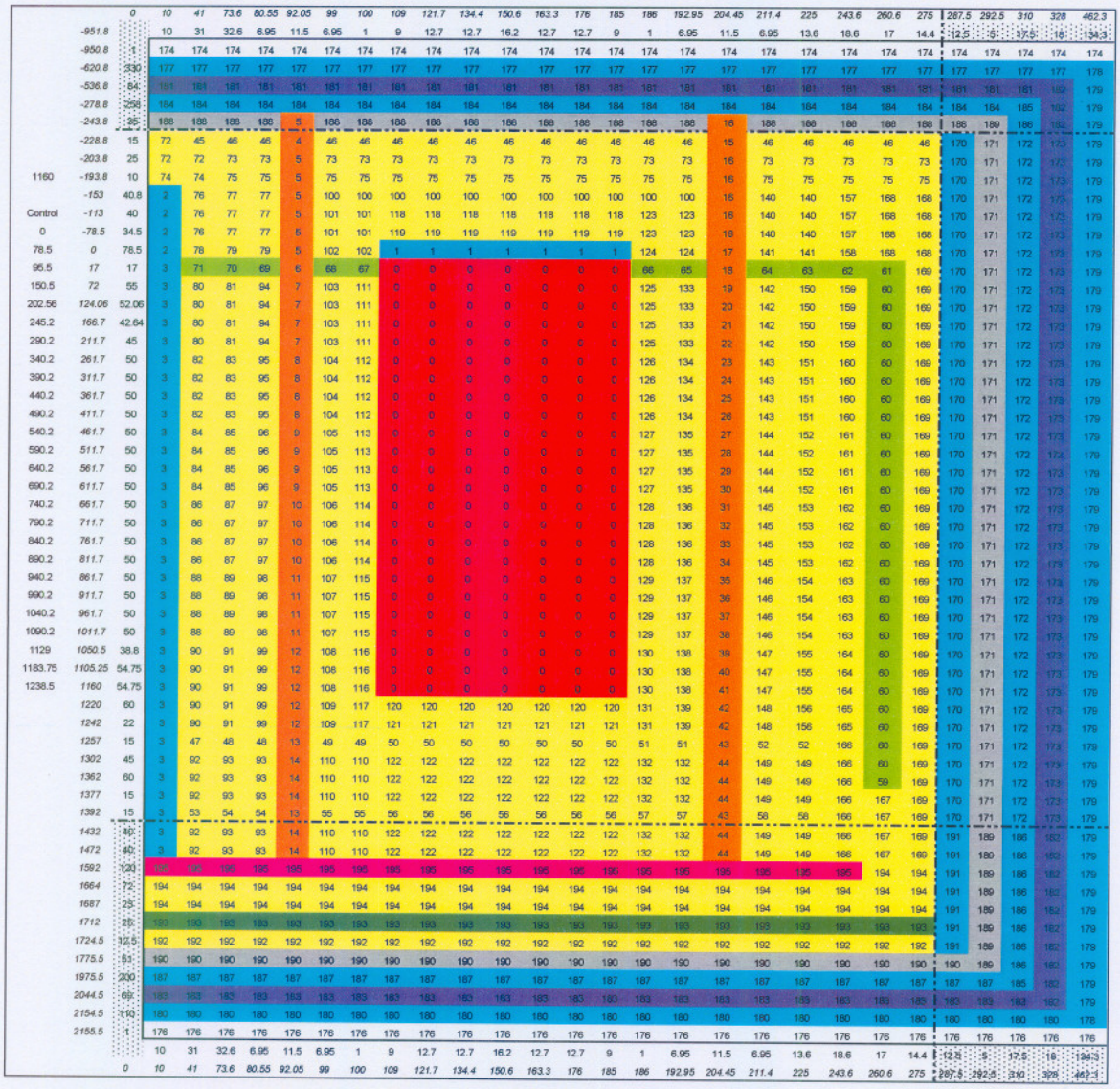

Figure 11: Region Layout for VSOP Calculations [24]

Table 3: Material Specification for the Batches of VSOP [23]

Region	Material
0	Fuel core
1	Upper Void Cavity
2-3	Central Hole
4-14	Reactor Shut Down System
15-44	Reactor Control System
45 – 58, 69 – 73, 76 – 99, 103 – 169, 192, 194	Graphite
59 – 60	Riser
61 – 66	Helium Inlet
67, 68	Bypass flow to central column slits
74 – 75, 100 – 102	Bypass flow to central column
170 , 191	Gap
171 , 189	Core Barrel
172, 184 - 187	Gap
173, 181 – 183	RPV
174 – 176	Outer Boundary
177 – 180	Gap
188	Top Plate
190	Bottom Plate
193	Graphite
195	Outlet Plenum

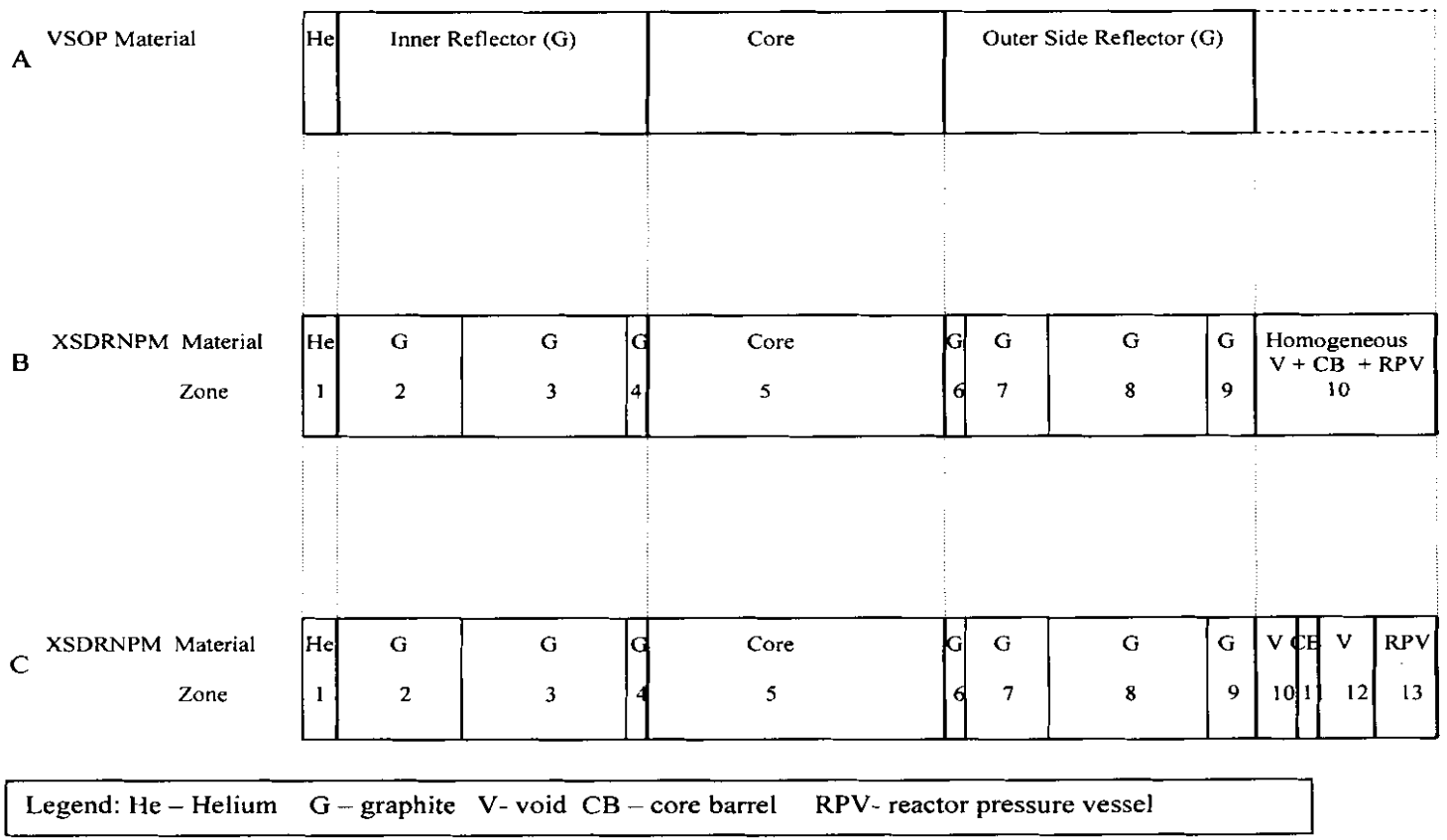

Figure 12: Material Assignment in the Radial Direction of the Reactor for the Different Geometrical Models Used

3.4 Calculational Methodology for α

In this section, the methodology used for the calculations performed and the analysis procedures are presented.

In summary, this involved

- Investigation of the origin of the alpha value of 0.4692 (default value in VSOP manual used in model V1.0.3) that is currently being used
- Investigation of the sensitivity of k_{eff} as a function of alpha in VSOP calculations.
- Aspects of the validity and other related issues of XSDRNPM for comparison with VSOP
- Determination of the value of alpha for use in the VSOP model, by using the transport code XSDRNPM, and including the heterogeneous core barrel and RPV in the calculation.
- Evaluation of the results of XSDRNPM calculations and comparison of the results of XSDRNPM with VSOP results. These comparisons will include other aspects like flux profiles, leakages, and the influence of the number of energy groups

The methodology regarding the third aspect above will be presented in chapter 4.

3.4.1 Investigation of the Origin of α = 0.4692

This was done mathematically, and the derivation was presented in chapter 2.2.3.

3.4.2 Determination of the Value of α for Use in the VSOP Model

This procedure involved a number of steps.

i. The reference input for XSDRNPM [26] was adapted so that the output contained the angular fluxes at each spatial mesh point.

ii. From this output, the partial currents were calculated using the equations

$$J_{+} = \sum_{m=1}^{24} \psi_m \mu_m w_m \ , \ \mu_m > 0 \tag{38}$$

$$J_{-} = \sum_{m=1}^{24} \psi_m |\mu_m| w_m \ , \ \mu_m < 0 \tag{39}$$

where μ_m and w_m were the quadrature cosines and weights respectively defined in XSDRNPM, and ψ_m were the angular fluxes at each quadrature.

In this model of XSDRNPM, the order of the quadrature was set to 8 which translated to 24 angular fluxes generated at each spatial position.

The calculations were done at the radial distance of 275 cm.

It should be noted that there were 238 energy groups defined in the XSDRNPM calculations, therefore 238 x 2 partial currents were calculated.

iii) The 238 x 2 partial currents were compressed into 4 x 2 partial currents.

This was done by using the superposition principle

$$J_k^{\pm} = \sum_{i=NL(k)}^{NU(k)} J_i^{\pm} \quad k = 1,2,3,4 \tag{40}$$

where $NL(k)$ and $NU(k)$ defined the lower and upper limit of the energy group number in XSDRNPM that corresponds to the energy group boundaries of the VSOP group k. These numbers $NL(k)$ and $NU(k)$ are listed in Table 4.

iv) Once J. and J+ were calculated at the point in question, α was determined using eq 37 for the four energy groups.

v) In order to determine the weights of each group, the adjoint transport equation was solved using XSDRNPM, where, instead of calculating the fluxes at each position, the importance function was calculated. The importance functions calculated in the 238 energy groups were then collapsed into four groups according to the scheme shown in

Table 4, and these four importances with their sum normalized to 1 were used as the weighting functions.

vi) The 4 alpha values calculated in iv) above were finally collapsed into a single value using the equation

$$\overline{\alpha} = \sum_{i=1}^{4} w_i \alpha_i \tag{41}$$

where w_i are the weights in each energy group.

Table 4: Energy Group Compression Scheme for XSDRNPM

VSOP group	$NL(k)$	$NU(k)$	Lower energy boundary (eV)	Upper energy boundary (eV)
EG1	1	44	$1.1\text{x}10^5$	$1.0\text{x}10^7$
EG2	45	116	29.0	$1.1\text{x}10^5$
EG3	117	161	1.86	29.0
EG4 (thermal)	162	238	0.001	1.86

3.4.3 Evaluation of XSDRNPM Calculation Results and Comparison with VSOP Results

To do this, applicable scalar fluxes were extracted from the XSDRNPM and VSOP outputs, depending on the comparison being done. The differences used were always in relation to the reference case, i.e., the % difference for observable Y_i was calculated as

$$\%diff = 100 \times \frac{Y_i - Y_{ref}}{Y_{\max}} \tag{42}$$

where $Y_{\max}$ is the maximum flux of the reference case.

3.5 Model Adjustments and Code Running Practicalities

3.5.1 VSOP

3.5.1.1 Running of VSOP

VSOP was run on a PENTIUM IV desktop personal computer using a DOS prompt under Windows with the following script file.

```
vsop99_3-jul04-ms p400-s.fil
vsop99_3-jul04-ms p400-e.fil
vsop99_3-jul04-ms p400-t.fil
vsop99_3-jul04-ms p400-t2.fil
vsop99_3-jul04-ms p400-t3.fil
vsop99_3-jul04-ms p400-ee.fil
```

The .fil files contain the file names of the input and output files, restart files and library files for each time that VSOP was run in the above sequence. These .fil files are listed in Appendix B.

Because the input files are extremely long, they are not included in this report. However, [24] [25] give a detailed description of the parameters that are used in the input.

The above sequence of VSOP runs is done so that the calculation proceeds according to the following scheme.

i. Calculation of the geometry and initial loading of the fuel.
ii. Calculation of the neutronics without thermal hydraulic feedback to the core but with actual recirculation of fuel and guessed temperature.
iii. Calculation of the neutronics with thermal hydraulic feedback, so that the core proceeds to equilibrium (3 runs).
iv. Final calculations to produce desired output.

3.5.1.2 Input File Changes in VSOP

To change the alpha value in the VSOP calculations involved changing parameter XMISI of card C10 of input file p400-s.i. α was set to have a range of values between 0.0500 and 0.4692.

3.5.2 XSDRNPM

3.5.2.1 Running of XSDRNPM

XSDRNPM was run on a PENTIUM IV desktop personal computer using a DOS prompt under Windows using the command

SCALE44 filename

The output was automatically written to filename.o

3.5.2.2 Reference Input File for XSDRNPM

The reference input file [26] was used as the basis for determining the partial currents. It was however modified to suit the requirements for the present study. Information regarding this model is found in [27] [28]. This reference case was chosen because the angular fluxes could be calculated at the required point of the VSOP boundary position. Further, although the XSDRNPM model is a 1-d model, this model represents the radial cross section through the center of the VSOP model and is therefore adequate.

3.5.3 Input Files for XSDRNPM and Model Changes

The following adaptations were necessary in the input file.

i) Changing IDI to 1 of line 2$ to enable printing of angular fluxes.

ii) Changing IGMF to 4 of line 4$ to increase the number of energy groups in the collapsed sets to 4 to match that of the VSOP input model.

iii) Changing line 51$ as a necessary change because of changing IGMF.

iv) Changing IZM from 10 to 13 of line 1$ where IZM is the number of separate material zones. Figure 12B shows the assignment of regions in the reference model. Here, the outer boundary of the side reflector was at the right-hand edge of zone 9 and radially at position 275 cm. The region from this outer boundary of the side reflector to the outer boundary of the RPV was then specified as zone 10. Thus, zone 10

was a homogenous region consisting of void, core barrel and RPV extending radially from 275 cm to 328 cm.

For the adapted model used in this study, zone 10 was split up into four zones 10, 11, 12 & 13. Figure 12C shows this assignment. Therefore, the core barrel, which is zone 11, extends from 287.5 cm to 293.5 cm and the RPV, which is zone 13, extends from 310.0 cm to 328.0 cm. The helium voids are zones 10 and 12.

For comparison, the material assignment in VSOP is shown in Figure 12A. It is noted that this ends at 275.0 cm.

v. Changing IM of line 1$ because of the redefinition of the zones.
vi. Changing the 7^{th} entry of line 15* because zones 10 to 13 are now heterogeneous.
vii. Changing lines 35* and 36$ because the number of zones were increased from 10 to 13.

It should be further noted that the right boundary of the VSOP model at 275 cm is not a boundary point of the XSDRNPM model. In the XSDRNPM model, this position is within the spatial mesh of the neutronic analysis. The boundary of the XSDRNPM model is at 328 cm, and was defined as a vacuum boundary condition.

In order to do an adjoint calculation in XSDRNPM, the parameter ITH was changed to 1 of line 1$ in the input file.

3.5.3.1 Extraction of Data From XSRDNPM Output Files

The angular flux data that was written to the output file from XSDRNPM could not be easily manipulated by simply copying over to a spreadsheet, like those in Microsoft Excel. Therefore, a utility program was written to extract this data. Further, the partial currents were calculated according to eq 38 and eq 39. The listing of the source code for this program is given in Appendix C.

4. Initial Studies with XSDRNPM and VSOP

It has been mentioned that in the model of VSOP, the CITATION calculation ends at the outer edge of the side reflector, which is at 275 cm from the centre, with the assumption that a void exists beyond the side reflector, and that the main objective of this study is to obtain a correct value for α.

However, a few questions arise that need to be answered before accepting the α value calculated. One of these questions concerns the validity of the XSDRNPM results for use in VSOP.

This and other questions will be presented in this chapter.

4.1 XSDRNPM Cases and Results

For easy reference, all the cases run in XSDRNPM and used in the discussions in this chapter are listed in Table 5 with the k_{eff} results given in Table 6. The discussion of these results and cases will follow in the rest of the chapter. (See section 3.5.3 for the specific changes made to the input files).

Table 5: Description of XSDRNPM Input Cases

Case	Description of Changes	Effective Change
1	Same as input file pbmr-a-o, [26] with changes made to bring output to required form	Output Presentation
2	Region from x = 275 cm to 328 cm is composed of 4 heterogeneous zones 10, 11, 12 & 13. Zones 10 and 12 are helium void of thicknesses 12.5 cm and 16.5 cm. Zone 11 is the core barrel with thickness 6 cm. Zone 13 is the RPV with thickness 18 cm.	Outer region changed from homogeneous to heterogeneous

Case	Description of Changes	Effective Change
3	This is the same as case 1. The difference is that the mesh spacing is changed to match those of VSOP.	Mesh spacing
4	This is the same as case 2. The difference is that the mesh spacing is changed to match those of VSOP.	Mesh spacing
5	This is the same case 4. The difference is that the core barrel thickness is set at 5 cm.	Core Barrel Thickness
6	The flux calculation ends at 275 cm. An albedo boundary is used at this position corresponding to $\alpha = 0.1141$, entered in the input file at line 47*. With the albedo defined in the usual way as J_-/J_+, the albedo can be determined using eq 36 of Chapter 2.4, giving the result 0.627075.	$\alpha = 0.1141$
7	The flux calculation ends at 275 cm. The void boundary condition is used.	$\alpha = 0.4692$

Table 6: K_{eff} for the Various XSRNP Calculations

Case	k_{eff}	$\Delta\rho = \frac{1}{k_7} - \frac{1}{k_\#}$ (pcm)
1	1.04158	427
2	1.04158	427
3	1.04158	427
4	1.04154	423
5	1.04148	418
6	1.03933	219
7	1.03697	0

4.2 Establishing whether an Accurate Value of α is necessary

The first question is to establish whether it is necessary to calculate a correct value for α, or in other words, if the results are sensitive to changes in α. To answer this question, calculations using VSOP and XSDRNPM were done. For each set of calculations the boundary conditions were changed, and the effect on the reactivity was noted. In VSOP, this amounted to running the code with α values ranging from 0.05 to 0.4692. The larger value ($\alpha = 0.4692$) represents a vacuum boundary condition while the lower value (0.05) was an arbitrary choice. In XSDRNPM, it meant redefining the region of interest in the analysis, so that the geometrical model ends in a void boundary condition at 275cm, the outer boundary of the side reflector.

4.2.1 Reactivity Effects

The resulting k_{eff}, and change in reactivity ρ from the VSOP sensitivity study of α are listed in Table 7, where ρ is defined as

$$\rho = 10^5 \times \left(\frac{1}{k_{crit}} - \frac{1}{k_{eff}} \right), \qquad k_{crit} = 1 \qquad [pcm]$$

Figure 13 plots the reactivity changes as a function of α. As can be seen from this graph, the change in reactivity is quite significant for α less than 0.3. (Reactivity effect larger than 50 pcm was considered to be meaningful). Therefore it is concluded that the correct value of α should be determined, and if it is found to be less than 0.3, then α must be corrected for future models and calculations.

When the sensitivity of α was tested in XSDRNPM, the k_{eff} for the case corresponding to $\alpha = 0.4692$ (Case 7) was compared with the case corresponding to $\alpha = 0.11414$ (Case 6). It is seen from Table 6 that the change in reactivity is 219 pcm, which is significant. Comparing this with similar VSOP results ($\alpha = 0.11414$) shows a fairly good agreement (249 pcm). The results confirm that the reactivity can change significantly with changes in α and that the correct α value must be determined.

Table 7: VSOP Reactivity as a Function of α

α	k_{eff}	ρ (pcm)
0.0500	1.0060	596
0.1000	1.0030	299
0.1146	1.0025	249
0.1500	1.0018	180
0.2000	1.0011	110
0.2500	1.0008	80
0.3000	1.0005	50
0.3500	1.0003	30
0.4000	1.0002	20
0.4692	1.0000	0

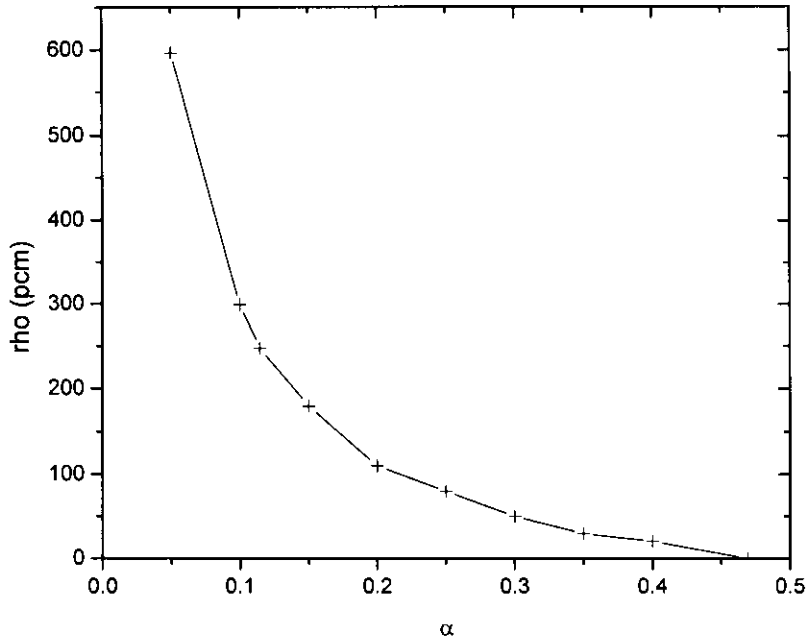

Figure 13: Reactivity Effects for Different Boundary Conditions

4.2.2 Effect of α on Leakages

It is also worthwhile considering the influence α has on the leakages in the VSOP calculations. The leakage is defined as the fraction of neutrons that leave the volume per lost neutron, noting that neutrons can also be lost by absorption in the volume. This fraction is expressed as a percentage. A negative leakage means that neutrons enter into the volume. These leakages are listed in Table 8.

As can be seen from the last row of the table, the total leakage shows a change of 0.41%, to which the thermal group makes the largest contribution. We can correlate this with the change in reactivity as shown in Table 7, since leakage should influence the criticality of the reactor. Thus, a change in reactivity of 596 pcm should correlate with a change in leakage out of the core of 0.41%.

Table 8: VSOP Leakages out of the Core of the Four Energy Groups as a Function of α (Expressed as a Percentage)

α	$leak_1$	$leak_2$	$leak_3$	$Leak_4$	$leak_{tot}$
0.0500	21.29	12.40	0.27	-19.19	14.77
0.1000	21.28	12.40	0.27	-18.97	14.98
0.1146	21.27	12.40	0.27	-18.93	15.01
0.1500	21.27	12.40	0.27	-18.88	15.06
0.2000	21.27	12.40	0.27	-18.84	15.10
0.2500	21.27	12.40	0.27	-18.81	15.13
0.3000	21.26	12.40	0.27	-18.79	15.15
0.3500	21.26	12.40	0.27	-18.78	15.16
0.4000	21.26	12.40	0.27	-18.77	15.17
0.4692	21.26	12.40	0.27	-18.76	15.18
Maximum difference	-0.03	0.00	0.00	0.43	0.41

4.3 Validity of using a Single Value for α in VSOP

In VSOP, only a single α value can be given as input. The question arises whether this is sufficient, or whether four albedo values should be entered corresponding to the four energy groups.

A further approximation is also introduced since a full albedo matrix, with terms representing slowing down and upscattering, is in fact needed to represent the true response of the system.

To study this, two cases that try to represent this effect were defined in XSDRNPM. In case 2, the neutronic boundary condition is defined at 328 cm, so in effect this means that the correct neutronic response is modelled at

position 275 cm in 238 energy groups. In case 6, the boundary condition is set at 275 cm, with an albedo boundary condition set to 0.627075, which is equivalent to $\alpha = 0.1141$, i.e., only a single group boundary condition value exists. The k_{eff} values are listed in Table 6 and the change in reactivity is 208 pcm, which is considered significant. Therefore, using a single α as compared to a full albedo boundary condition matrix has a significant effect on the reactivity.

Figure 14 plots the fluxes of these two cases. This figure consists of four rows of three plots. Each row represents one of the four energy groups, the first (i.e., top) row being the first energy group, the 2nd row being the 2nd energy group, the 3rd row being the 3rd energy group, and the 4th row (bottom row) being the thermal energy group.

Each row contains three plots. The content (i.e., the spectra) of each of these three plots in a given row is identical. The difference between these plots lies in the x axis scale. The left plot is from 0 cm to 50 cm, the centre plot is from 0 cm to 350 cm, and the right plot is from 260 cm to 340 cm. Thus, the centre plot displays the entire radial length of the core up to the outer edge of the RPV (which ends at 320 cm). The left plot is a magnification of the inner part of the spectrum, and the right plot is a magnification of the outer part of the spectrum. This was done so that the fine details of the spectra can be highlighted while keeping the complete spectra in focus. This same representation will be used later in this chapter for Figure 15 - Figure 17.

The differences in fluxes are listed in Table 9 for positions x = 0 cm and x = 275 cm. The differences were calculated using the maximum flux (in the group) as relative value according to eq 42. While the three epi-thermal spectra do not show any significant differences, the thermal group does.

Table 9: % Flux Differences between Case 2 and Case 6 as a Ratio to the Maximum Flux in each Energy Group at Positions 0 cm and 275 cm

X position	EG1	EG2	EG3	EG4
0.00	0.00	0.00	0.00	-4.6
275.00	-0.00	0.00	0.01	-2.1

We can conclude that the use of a simple albedo boundary condition (or single α value) can not accurately conserve the thermal neutron flux at the boundaries and is thus not adequate to represent the neutronic behaviour at the boundary. The effect of this approximation is largely restricted to the thermal group and with the large differences only seen in the central reflector (x = 0 – 50 cm) and close to the outer boundary. However, it must, be noted that the importance of this effect might be overemphasized by the 1-D model and the use of the 238 group calculation as reference.

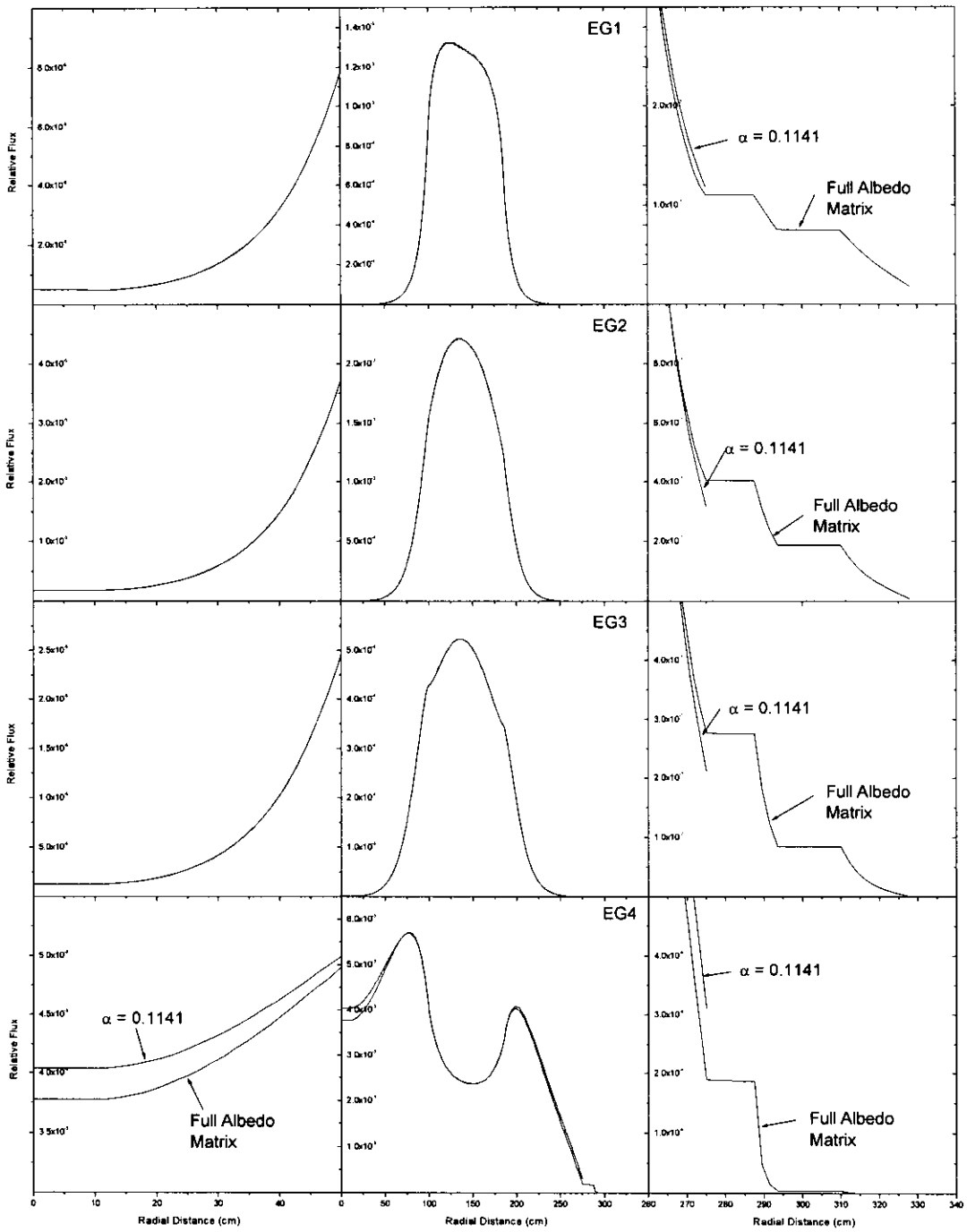

Figure 14: Comparison of Fluxes between a Single α (α = 0.1141) and a Full Albedo Matrix (Cases 4 and 6)

4.4 Defining the Core Barrel and Reactor Pressure Vessel as Homogenous or Heterogeneous

The next question that will be addressed is whether defining the outer structures (core barrel – void – reactor pressure vessel) as heterogeneous or homogeneous will affect the reactivity. Case 1 is homogeneous and case 2 represents the heterogeneous case (see Table 5). The k_{eff} values and change in reactivity shown in Table 6 is insignificant.

4.5 Mesh Size Effects in XSDRNPM

The reference model of VSOP and the reference model of XSDRNPM do not have the same mesh sizes in the radial direction. Therefore, it was necessary to change the mesh sizes of XSDRNPM to match those of VSOP. The question then arose whether there would be a significant difference in the change in reactivity when this was done.
In Table 5, cases 1 and 3 are the same except for the mesh size that was changed, as in cases 2 and 4. From the results listed in Table 6, it can be seen that the change in reactivity is not significant.

When the fluxes are compared in Figure 15, for the two homogeneous cases no visible differences can be seen (lines overlay each other). This means that making the mesh sizes slightly smaller or increasing the number by a small amount will not show any differences.

Figure 16 shows the same comparison but this time for the two heterogeneous cases. Now small differences can be observed as shown in Table 10. These difference are considered to be negligible.

Table 10: % Flux Differences between Cases 2 and 4 as a Ratio to the Maximum Flux of each Energy Group at Positions 281.25 cm and 300.57 cm

Position (cm)		Groups			
		EG1	EG2	EG3	EG4
	max flux	0.0013	0.0022	0.0005	0.0057
281.25	% diff	0.0000	0.0000	0.0000	-0.0525
300.57	% diff	0.0000	0.0001	0.0004	0.0299

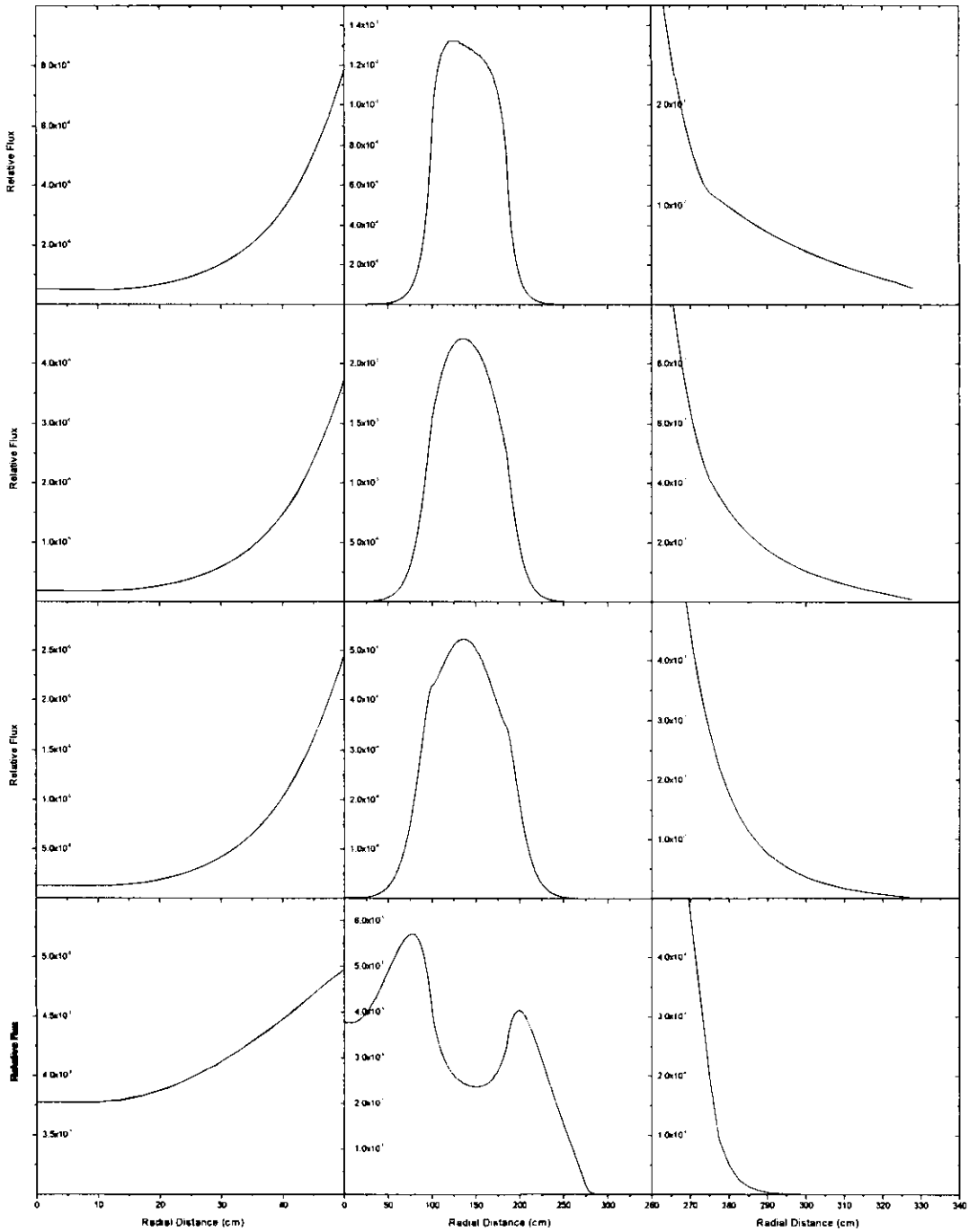

Figure 15 Comparison of Fluxes for the Homogeneous Model with different Mesh Spacing (Cases 1 and 3)

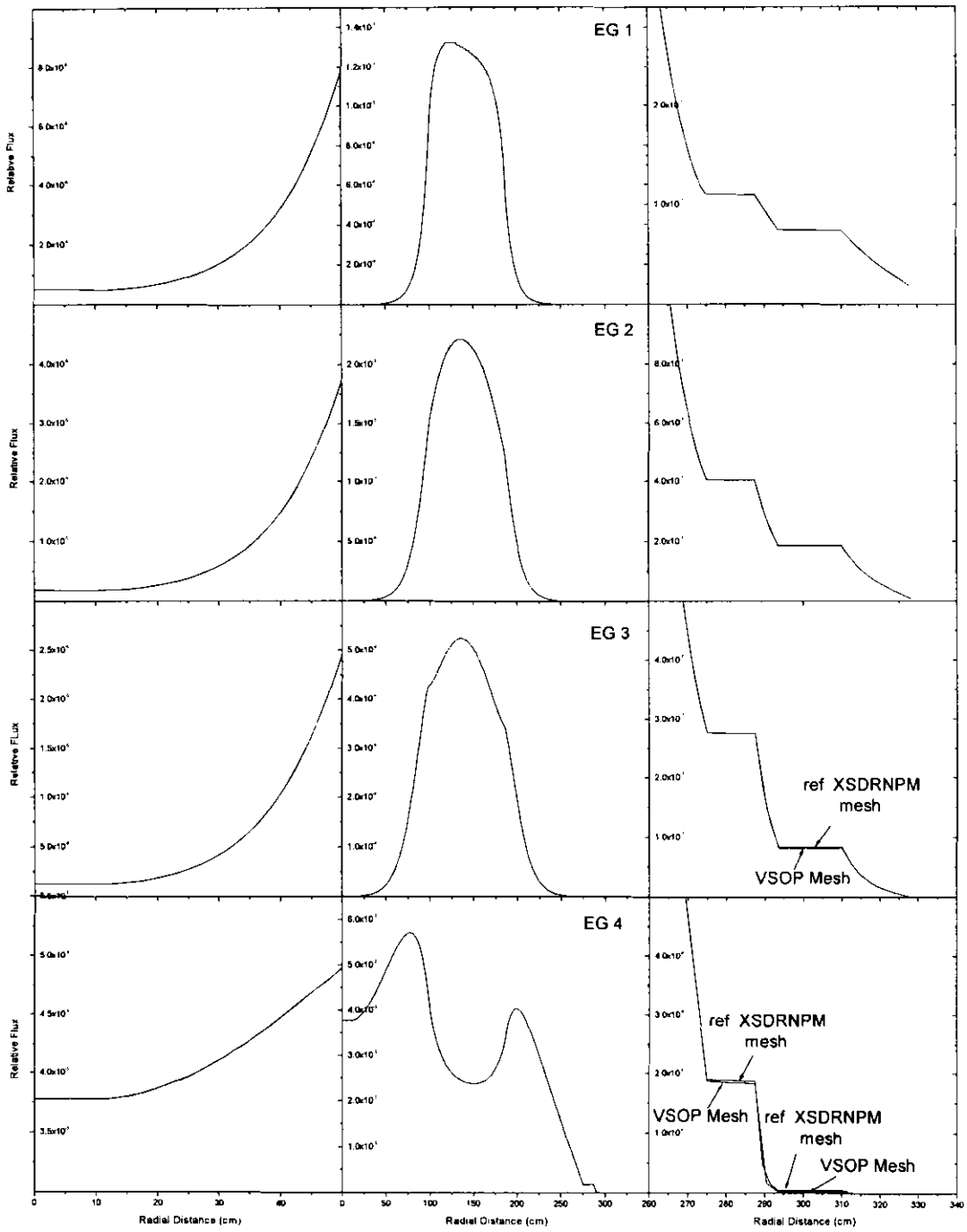

Figure 16: Comparison of Fluxes for the Heterogeneous Model with different Mesh Spacing (Cases 2 and 4)

4.6 Changing the Core Barrel Thickness from 6 cm to 5 cm

In an earlier model of the PBMR reactor, the core barrel was set at 5 cm. In this study the core barrel was set at the current design value of 6 cm. Therefore, it was decided to study the effect of decreasing this core barrel width back to 5 cm using XSDRNPM.

Case 5 is the same as case 4 with the core barrel thickness decreased (see Table 5). The change in reactivity of only 5 pcm is considered insignificant (see Table 6). The flux differences are shown in Figure 17. A thicker core barrel will absorb more neutrons so that in the region immediately beyond the core barrel, the flux in the 5 cm core barrel case should be larger than the flux of the 6 cm core barrel case as observed. The percentage difference between the two calculations as a ratio of the maximum flux (according to eq 42) at the radial position 300.57 cm is listed in Table 11. The differences are small and this means that the change in the core barrel thickness of 1 cm will not significantly affect the calculated value of alpha.

Table 11: % Flux Differences between Cases 4 and 5 as a Ratio of the Maximum Flux in each Energy Group at Position 300.57 cm

Position (cm)	EG1	EG2	EG3	EG4
300.57	-0.0003	-0.0010	-0.0032	-0.0748

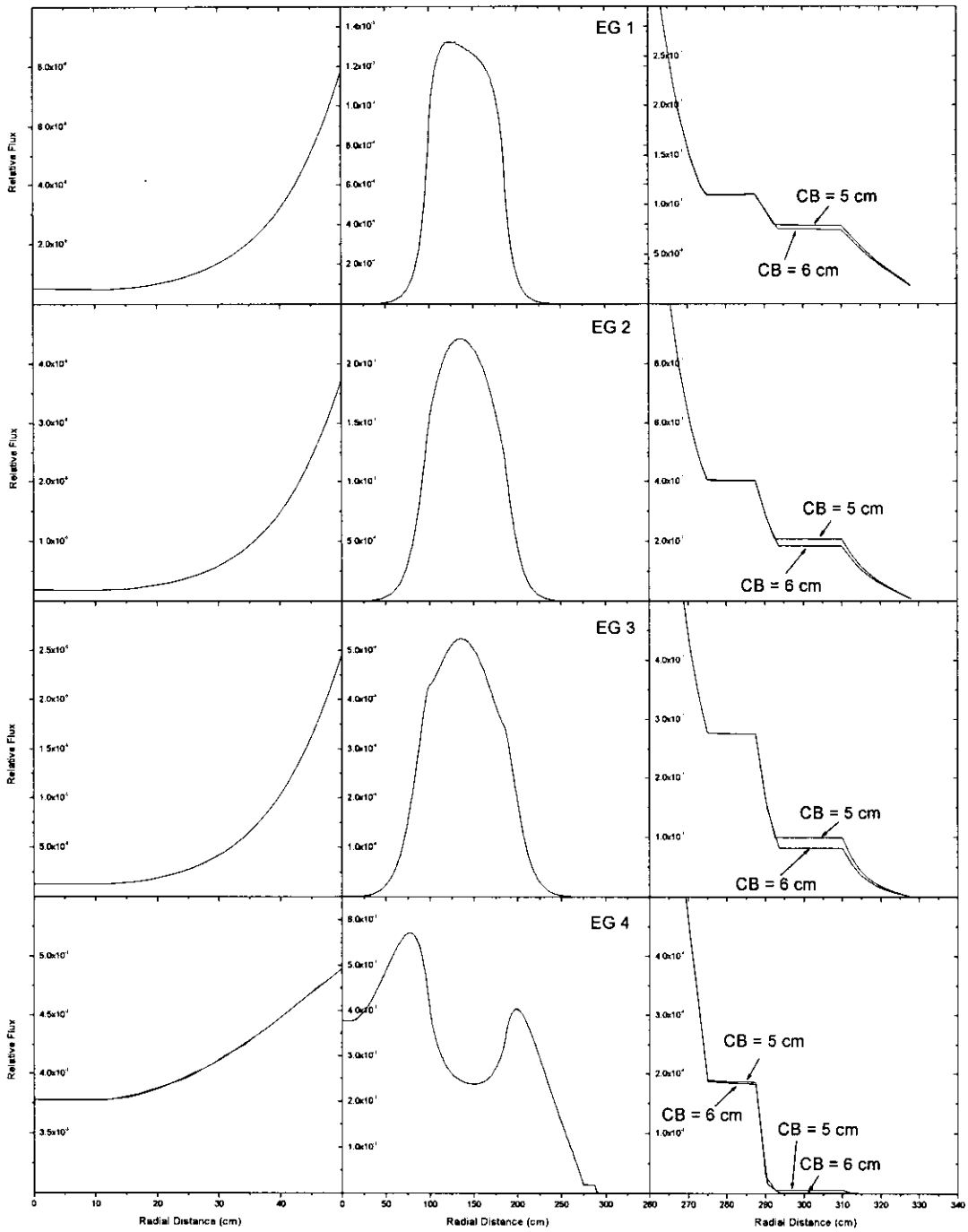

Figure 17: Comparison of Fluxes between Two Core Barrel Thicknesses (Cases 4 and 5)

4.7 Comparison of Fluxes using Albedo and Void Boundary Conditions

In section 4.4, the cases 1 and 2 were presented, in which the boundary was set a 328 cm, which effectively meant a reference albedo boundary matrix at 275 cm. Case 1 has the homogeneous representation while case 2 has the heterogeneous representation of the CB and the RPV.

In section 4.3, and single albedo value corresponding to $\alpha = 0.1141$ was defined at 275 cm (Case 6) while in section 4.2 a void boundary condition was set (Case 7). Flux profiles for these four cases are shown in Figure 18. The XSDRNPM flux was scaled to that of the VSOP flux by multiplying the XSDRNPM flux by a constant so that the sum of the least square differences between the two fluxes was a minimum.

The differences are visually notable in the outermost radial positions for all energy groups. The heterogeneity of case 2 and the homogeneity of case 1 is clearly visible.

The flux behaviour at position 275 cm is as expected, being smaller for the vacuum condition (Case 7) as compared with $\alpha = 0.1141$ (Case 6). Noticeable differences can also be observed in the thermal flux in the centre of the central flux (x = 0 cm). The percentage difference between individual fluxes and the average flux for each group, as a ratio of the maximum flux, is listed in Table 12 for the positions at x = 0 cm and x = 275 cm. From this it is seen that only the differences in flux of the thermal energy group are significant. There is good agreement in the fluxes between the different cases for energy groups 1, 2 and 3.

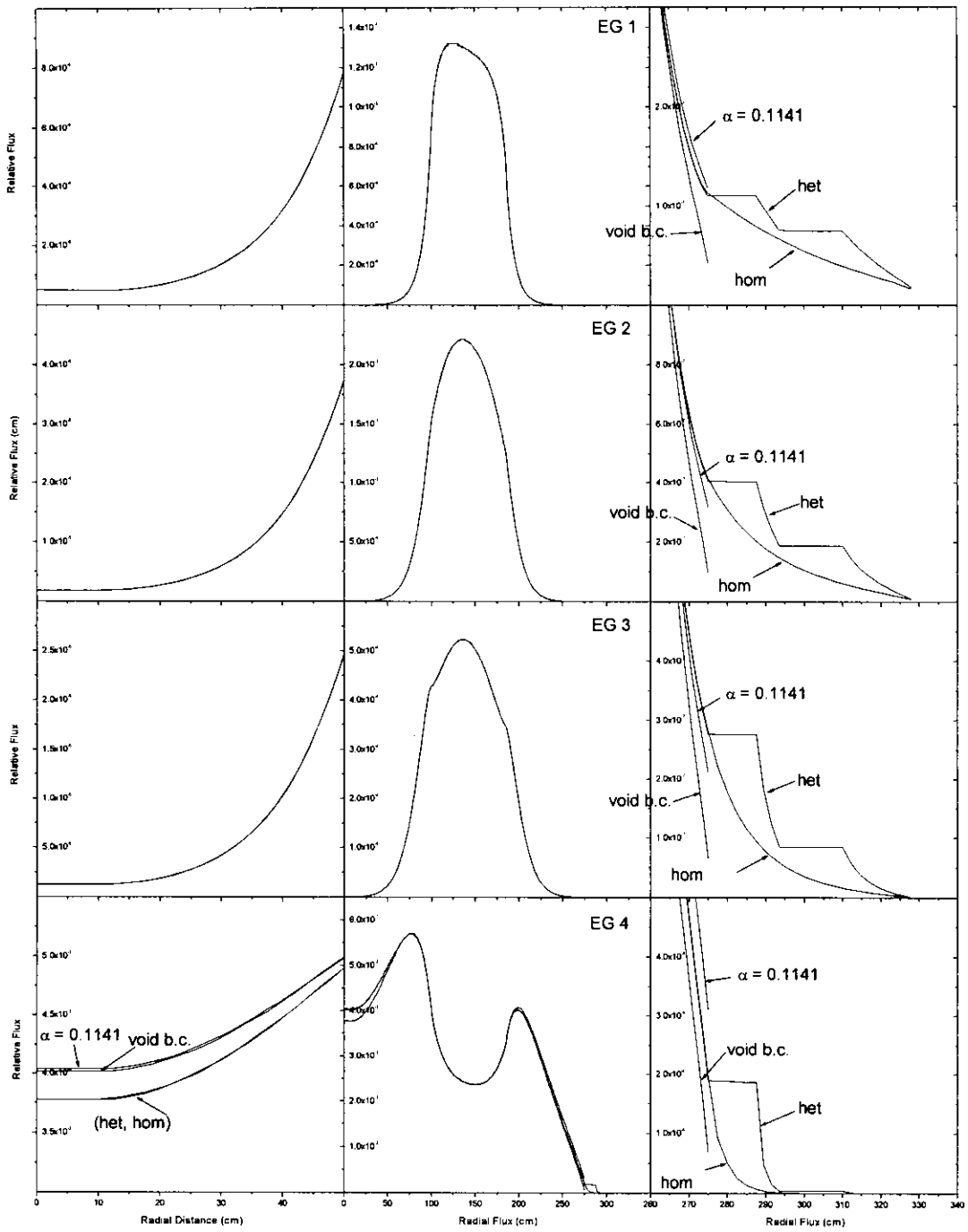

Figure 18: Comparison of Fluxes between Homogeneous, Heterogeneous, Void Boundary Condition and α = 0.1141 (Cases 3, 4, 6 & 7)

Table 12: % Flux Differences between Cases 1, 2, 6 and 7. The Average of these Four Cases Expressed as a Ratio to the Maximum Flux in Each Energy Group at Positions 0 cm and 275 cm

Position		Individual Fluxes				Average	Max
(cm)		Case 1	Case 2	Case 6	Case 7	Flux	Flux
	EG1						
0		5.18E-7	5.18E-7	5.16E-7	5.17E-7	5.17E-7	0.00132
	% diff	0.00	0.00	-0.00	0.00		
275		1.13E-7	1.10E-7	1.18E-7	4.21E-8	9.58E-08	0.00132
	% diff	0.0	0.0	0.0	-0.0		
	Eg2						
0		1.86E-6	1.86E-6	1.86E-6	1.86E-6	1.86E-6	0.00221
	% diff	0.0	0.0	0.0	0.0		
275		4.14E-7	4.06E-7	3.17E-7	9.43E-8	3.08E-7	0.00221
	% diff	0.0	0.0	0.0	-0.0		
	Eg3						
0		1.28E-6	1.28E-6	1.28E-6	1.28E-6	1.28E-06	0.00052
	% diff	0.0	0.0	0.0	0.0		
275		2.82E-7	2.77E-7	2.12E-7	6.46E-8	2.09E-07	0.00052
	% diff	0.0	0.0	0.0	-0.0		
	Eg4						
0		0.0038	0.0038	0.0040	0.0040	3.91E-03	0.00571
	% diff	-2.2	-2.2	2.4	2.0		
275		1.98E-4	1.90E-4	3.10E-4	6.83E-5	1.92E-04	0.00571
	% diff	0.1	-0.0	2.0	-2.2		

4.8 Boundary Flux Evaluation using α in VSOP

In VSOP, the coarse meshes used to spatially define the reactor core are further divided into fine meshes. The flux values that are printed in the output of VSOP are the values calculated at the centre of the fine meshes. Eq 15 gives the formulation of α, where the flux and the gradient of the flux should be calculated at the edge of the mesh point, i.e., at r = 275.0 cm.

The question then arises whether VSOP evaluates the flux at this point or at the centre of the mesh. To answer this question, the following heuristic investigation was carried out.

Four cases were constructed, in which the number and sizes of coarse meshes and fine meshes immediately to the left of the r = 275.0 cm boundary were changed. These mesh configurations are shown in Figure 19.

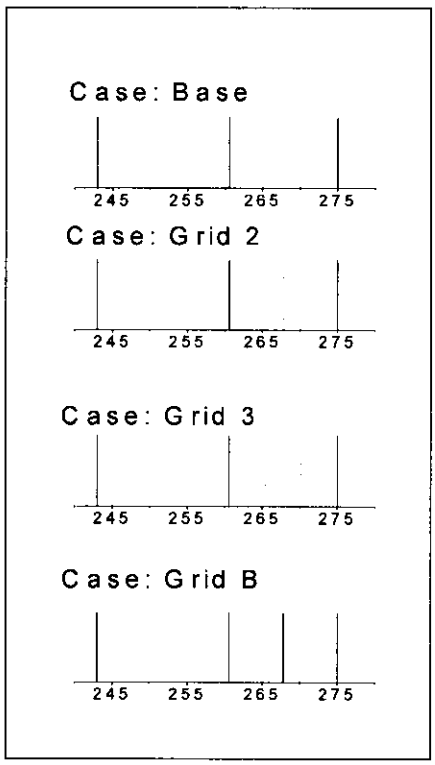

Figure 19: Positions of Meshes in the Outer Boundary

The flux values at the associated radial points as calculated by VSOP for each case are listed in Table 13 and plotted in Figure 20 A - D. Figure 20 E is the plot of all the data. The last flux point from each of the plots Figure 20 A – D forms a linear progression in Figure 20 E.

Table 13: Fluxes at Mesh Points in VSOP Calculations

Mesh Point	Flux (n/cm^{2}s)			
(cm)	Bases	Grid2	Grid3	Gridb
252.24	5.27E+10	5.54E+10	5.11E+10	5.54E+10
263.05			2.24E+10	
264.22				2.07E+10
264.27		2.05E+10		
267.9	1.13E+10		1.22E+10	
271.42				7.67E+09
271.47		7.62E+09		
272.65			5.78E+09	
278.3715	0	0	0	0

This linearity proves that eq 15 is evaluated on the mesh boundary, and that the flux point associated with this condition is at the midpoint of the last fine mesh, and not at the midpoint of the last coarse mesh.

To see this, suppose that the condition defined by eq 15 is taken to hold at the boundary position. Then depending on the size of the fine mesh Δ, the point ϕ_C of Figure 1 (section 2.2.3) will lie on the line extended from the points at $\phi = 0$ and ϕ_a. Since we have already shown in Figure 20E that for four different values of Δ, this is indeed the case, this means that the condition defined by eq 15 is applied at the boundary position.

If this condition was applied at the centre of the fine mesh, or the centre of the coarse mesh, and not at the right edge of the mesh, then the linear progression will not form as is seen in Figure 20E.

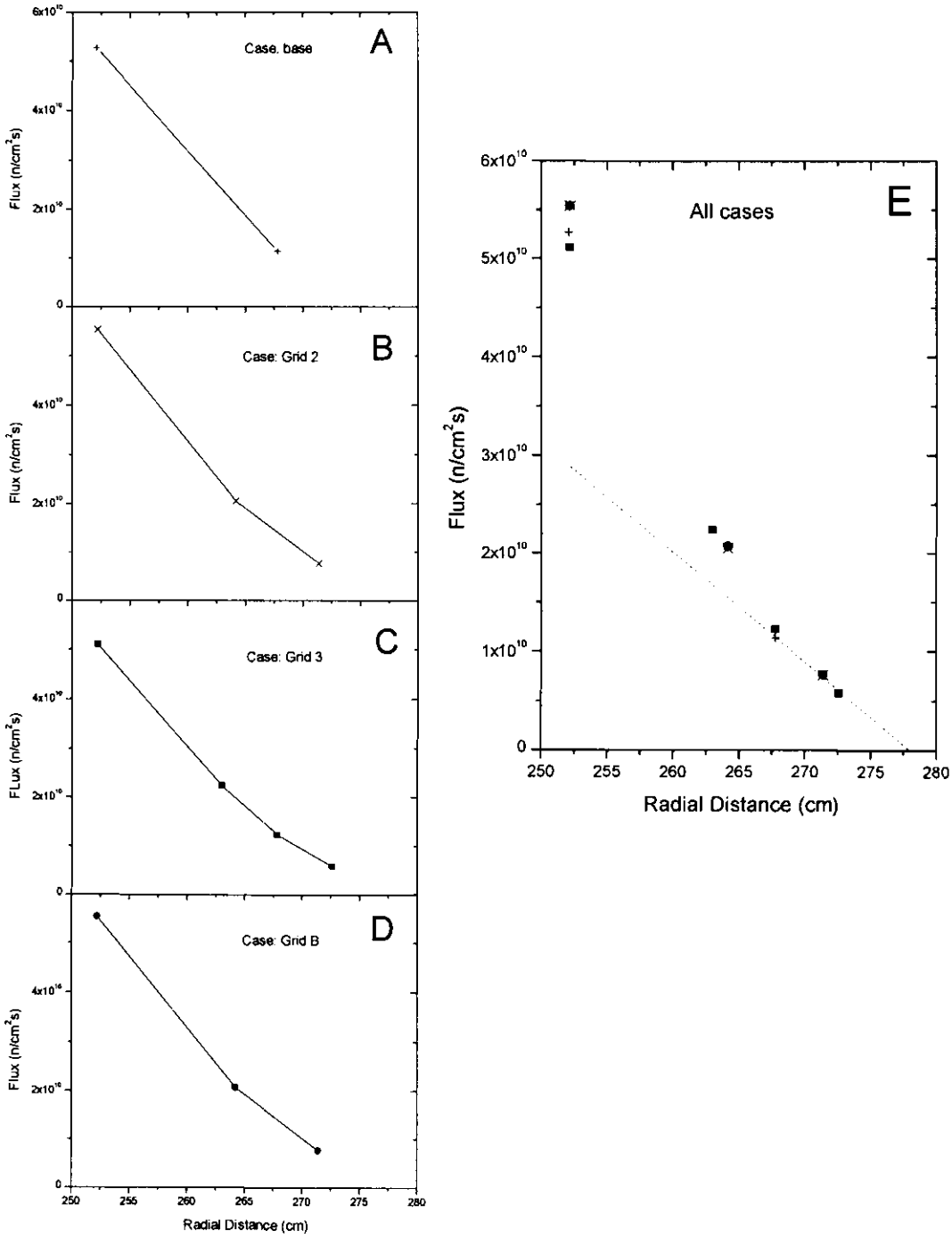

Figure 20: Fluxes at Mesh Points in the VSOP Calculations

5. EVALUATION OF α: CALCULATIONS, RESULTS AND DISCUSSION

In Chapter 4, studies showed that the accurate calculation of α is important and many model variations were performed to ensure that the best model is used to determine α for the problem under consideration. The 1-D transport solution from case 4, with meshes that correspond to VSOP and with the correct heterogeneous representation on the CB and RPV was used to derive α.

5.1 Evaluation of the Partial Currents J_- and J_+ at 275 cm

The partial currents at the chosen radial position (275 cm) were used to determine α as shown in chapter 2.4. The partial currents were calculated using eq 38 and eq 39 and since the XSDRNPM calculations are performed in 238 energy groups, 238 × 2 partial currents were obtained from the calculations.

5.2 Collapsing from Fine to Few Group Partial Currents

XSDRNPM calculates the flux spectra in 238 energy groups, whereas VSOP calculates the flux spectra in 4 energy groups. Thus, the 238 group partial currents obtained from XSDRNPM had to be collapsed to 4 group partial currents.

This was done by using the superposition principle:

$$J_k^{\pm} = \sum_{i=NL(k)}^{NU(k)} J_i^{\pm} \quad k = 1,2,3,4 \tag{43}$$

where $NL(k)$ and $NU(k)$ defined the lower and upper limit of the energy group number in XSDRNPM that corresponds to the energy group boundaries of the VSOP group k. These numbers $NL(k)$ and $NU(k)$ are listed in Table 14. The partial currents for the four energy groups are listed in Table 15.

Table 14: Energy Group Compression Scheme for XSDRNPM

VSOP group	$NL(k)$	$NU(k)$	Lower energy boundary (eV)	Upper energy Boundary (eV)
EG1	1	44	$1.1x10^5$	$1.0x10^7$
EG2	45	116	29.0	$1.1x10^5$
EG3	117	161	1.86	29.0
EG4 (thermal)	162	238	0.001	1.86

Table 15: Partial Currents Calculated from XSDRNPM output

Group	J_- n/cm^2s	J_+ n/cm^2s
1	2.11E-08	3.66E-08
2	9.03E-08	1.18E-07
3	6.02E-08	8.19E-08
4	3.10E-05	6.84E-05

5.3 Evaluation of α from the Partial Currents

With J_- and J_+ calculated, α was determined (using eq 37) for the four energy groups. At this point it is of interest to note that whereas J_- and J_+ are calculated using transport theory, α determined using eq 37 is the diffusion theory formalism. The calculated 4-group α values are given later (in Table 17) but before evaluating the results, how to calculate the single α value required by VSOP, needs to be considered.

5.4 Determination of a Single α Value

5.4.1 Governing Equation for the Calculation

Since only a single α value can be input into VSOP, the four α values calculated should be further collapsed to find a single value. This was done by

$$\overline{\alpha} = \sum_{i=1}^{4} w_i \alpha_i \qquad (44)$$

where w_i are the weights in each energy group.

It should be noted that one cannot argue that the 238 group J_- and J_+ partial currents calculated from the 238 energy groups of XSDRNPM could be compressed into a single α value by group collapsing only (using eq 43) without the need for additionally weighting functions (eq 44). (In this case, one would set $k = 1$, $NL(1) = 1$ and $NU(1) = 238$ of eq 43). While this would be true if VSOP was run using only a single energy group in CITATION, this does not hold for the four-group calculation. In the diffusion theory formulation, the four energy groups are coupled to each other by the scattering terms and the fission terms (e.g., eq 4.73 of [12]). The spatial boundary conditions and leakage terms are uncoupled and are specific to each group and therefore four α values should be calculated in principle, even if they end up being identical.

This can be further seen by studying the leakages. In Table 16 the leakages for spectrum zone 250 are listed. The values were calculated using the range of α values used before (in section 4.2). Spectrum zone 250 is the outermost zone that characterizes the side reflector corresponding to the axial height of the core; it is the zone to which the external boundary condition is applied. (It should be noted that these leakages represents the leakage through all the surfaces of the zone, and not only through the external boundary surface, and therefore negative leakages should not be surprising). As can be seen from this table, the leakages from each group are not the same, hence the flux and the derivative of the flux should not be the same for all the energy groups. Leakage from the thermal group in particular is about a factor 10 in magnitude larger that those of the other three groups. This implies that the α value should not be the same.
Therefore, the weighting function of eq 44 is necessary.

Table 16: Leakages of the Four Energy Groups of Spectrum zone 250 as a function of α

alpha	$leak_1$	$leak_2$	$leak_3$	$Leak_4$	$leak_{tot}$
0.0500	-1.223E-4	-2.567E-4	-1.603E-4	-3.417E-3	-3.957E-3
0.1000	-1.136E-4	-2.333E-4	-1.453E-4	-2.358E-3	-2.851E-3
0.1141	-1.118E-4	-2.291E-4	-1.426E-4	-2.214E-3	-2.697E-3
0.1500	-1.081E-4	-2.210E-4	-1.374E-4	-1.963E-3	-2.429E-3
0.2000	-1.042E-4	-2.134E-4	-1.325E-4	-1.757E-3	-2.207E-3
0.2500	-1.014E-4	-2.084E-4	-1.292E-4	-1.631E-3	-2.070E-3
0.3000	-0.993E-4	-2.047E-4	-1.268E-4	-1.546E-3	-1.977E-3
0.3500	-0.975E-4	-2.020E-4	-1.250E-4	-1.485E-3	-1.910E-3
0.4000	-0.961E-4	-1.999E-4	-1.236E-4	-1.44E-3	-1.859E-3
0.4692	-0.946E-4	-1.976E-4	-1.221E-4	-1.392E-3	-1.806E-3

5.4.2 Weights

In order to determine the weights of each group, the adjoint transport equation was solved using XSDRNPM, where, instead of calculating the fluxes at each position, the importance function was calculated. The importance function gives a quantitative indication of how the neutron population at a given position and energy adds to the criticality of the reactor [12], and therefore it was a good weighting parameter.

The importances calculated in the 238 energy groups were then collapsed into four groups according to the scheme shown in Table 14, and these four importances with their sum normalized to 1 were used as the weighting functions.

The weights, individual alphas and the weighted alpha are listed in Table 17.

Table 17: Partial currents, weights and α values

Group	Weights	α	$\overline{\alpha}$
1	0.36975	0.1346	
2	0.18909	0.0671	0.11414
3	0.28019	0.0762	
4	0.16096	0.1885	

The weighted value to be used in VSOP calculations is therefore 0.11414.

5.5 Determination of α Using an Alternate Weighting Scheme

An alternate method to determine α is to first determine the weights for the 238 energy groups, and then calculate α using

$$\overline{\alpha} = \sum_{i=1}^{238} w_i \alpha_i \tag{45}$$

In this case, the 238 fine energy groups of XSDRNPM were not collapsed into the four energy groups, but rather kept at 238 energy groups. The importances were then evaluated for these 238 groups, and normalized to yield the weights.

By this method, α was calculated to be 0.12509. Using this value in VSOP, k_{eff} was found to be 1.0022, resulting in a change of reactivity of 30 pcm from the case with $\alpha = 0.11414$. It was thus concluded that using this alternate weighting approach did not yield a significant change in reactivity.

5.6 Comparisons of k_{eff} with other Code Calculations

5.6.1 Comparison with MCNP

From Table 7 it can be seen that the change in reactivity in the VSOP calculations between $\alpha = 0.1141$ and $\alpha = 0.4692$ is 249 *pcm*. In another work, an MCNP study [29] was conducted in which the reactivity was calculated both with the core barrel and without the control barrel defined in the model. The change in reactivity was found to be 150 ± 40 *pcm*. Although the RPV

should have also been included, a comparison with these results nevertheless gives a good indication of the validity of the present result. The present result of 249 pcm is within two standard deviations of the MCNP result and also includes the effect of the RPV, which should lead to the large reactivity effect.

5.6.2 Comparison with XSDRNPM

The input for XSDRNPM was modified so that the neutronic calculation ended at 275 cm, with a vacuum boundary subsequently set up at this position. This therefore was simulating the calculation corresponding to $\alpha = 0.4692$ of the VSOP calculation. The k_{eff} observed was 1.039, with the subsequent change in reactivity being 219 pcm as compared to the case equivalent of $\alpha = 0.1141$. Although this is a one-dimensional transport calculation, it compares well with the value 249 pcm of VSOP, differing by only 30 pcm.

5.7 Conclusions

Determining the correct value for α was the main objective of this study, therefore it is important to state the conclusions obtained in this chapter. The α values calculated were 0.1346, 0.0671 and 0.0762 for the three epi-thermal groups, listed in order from highest energy group to lowest energy group. For the thermal group, this value was 0.1885. Using the adjoint solution to calculate group weighting functions a single α value of 0.11414 was determined.

The change in reactivity of the VSOP calculations from the void neutronic boundary condition to that in which the CB and RPV were included, compared well with similar results of XSDRNPM and MCNP. This leads to confidence in the evaluated value of α.

6. FURTHER RESULTS AND DISCUSSION: COMPARATIVE STUDIES BETWEEN XSDRNPM AND VSOP AND THE EXTRAPOLATION LENGTH

In addition to determining α, other related aspects of the solutions of XSDRNPM and VSOP were studied. These observations will be reported in this chapter.

6.1 Evaluating Alpha using an Alternate Approach

Instead of calculating α using eq 37, one can also use the following equation to calculate alpha.

$$\alpha = -\frac{D}{\phi_i}\left(\frac{\phi_i - \phi_{i-1}}{x_i - x_{i-1}}\right) \tag{46}$$

where the exact value is obtained in the limit when

$$x_{i-1} \to x_i . \tag{47}$$

Here x_i and x_{i-1} are neighboring points on the mesh.

Eq 46 is just eq 15 written in difference form. Using this with XSDRNPM, *i* is then the position at the boundary, and *i-1* is the position of the mesh point immediately to the left of the boundary. To study the α obtained by this alternative method and to test its sensitivity to the mesh, the XSDRNPM input files were modified for mesh sizes of 2.80 cm, 1.40 cm and 0.70 cm. The weighted alpha was then calculated using eq 46 and eq 44. The results of these calculations are shown in Table 18.

The results show a large dependence on the mesh size and clearly do not converge, with $|\alpha|$ increasing with decreasing mesh spacing. This means then that the decreased mesh spacing used is still not close to the limiting case (eq 47) and hence this is not a good method for calculating α. It is not as robust as the partial current method adopted in chapter 5. It is interesting to note that for the smallest mesh spacing the value approaches $\alpha = 0.1141$, as

determined before. This indicates that the method would possibly yield the same reference result if the meshes were refined further, and that the method could also be used as long as care is taken to refine the mesh adequately.

Table 18: Finite difference evaluation of α using the flux defined at XSDRNPM mesh points

Mesh spacing (cm)	$\frac{1}{\phi_i}\left(\frac{\phi_i - \phi_{i-1}}{x_i - x_{i-1}}\right)$				Weighted value
	EG1	EG2	EG3	EG4	
2.8	-0.1363	-0.1331	-0.1204	-0.0290	-0.0285
1.4	-0.2725	-0.2662	-0.2408	-0.0581	-0.0570
0.7	-0.5450	-0.5325	-0.4817	-0.1162	-0.1140
	Weights				
	0.3698	0.1891	0.2802	0.1610	

6.2 Comparison of Flux Profiles Calculated Using VSOP and XSDRNPM

A direct comparison of the fluxes obtained in the 1-D XSDRNPM and 2-D VSOP solutions does not make sense at first. The fluxes are differently normalized and the VSOP model does include the changes in geometry above and below the core. However, the 1-D XSDRNPM model represents an axial cut through the centre of the fuel region and since the core is tall (~ 11 m) the flux profiles at that position can at least be compared. This comparison can help in quantifying any errors made in the diffusion approximation compared to the reference transport solution, especially far from the core.

(It would have been possible to model the top of the core and the bottom of the core using XSDRNPM by changing the widths of the zones (and also the mesh definitions) thus yielding values for α at these axial positions as well. However these calculations were left for a later study).

Therefore, it is accepted that the flux profile will change axially because of the changing geometry and materials. Figure 21, Figure 22 and Figure 23 show the flux profiles evaluated using VSOP at various axial positions.

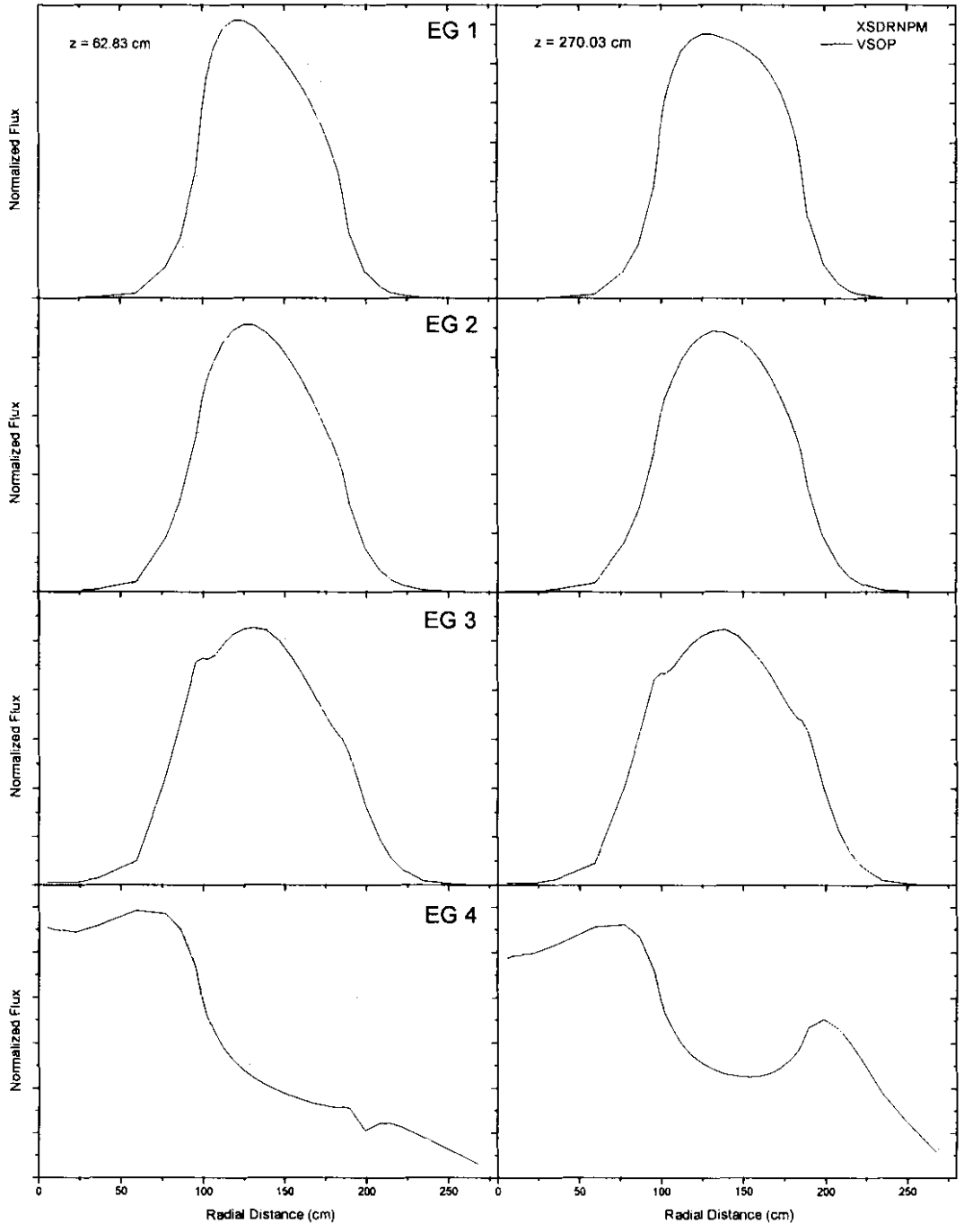

Figure 21: Four Group Radial Flux Profiles of VSOP and XSDRNPM at Axial Positions 62.83 cm and 270.03 cm.

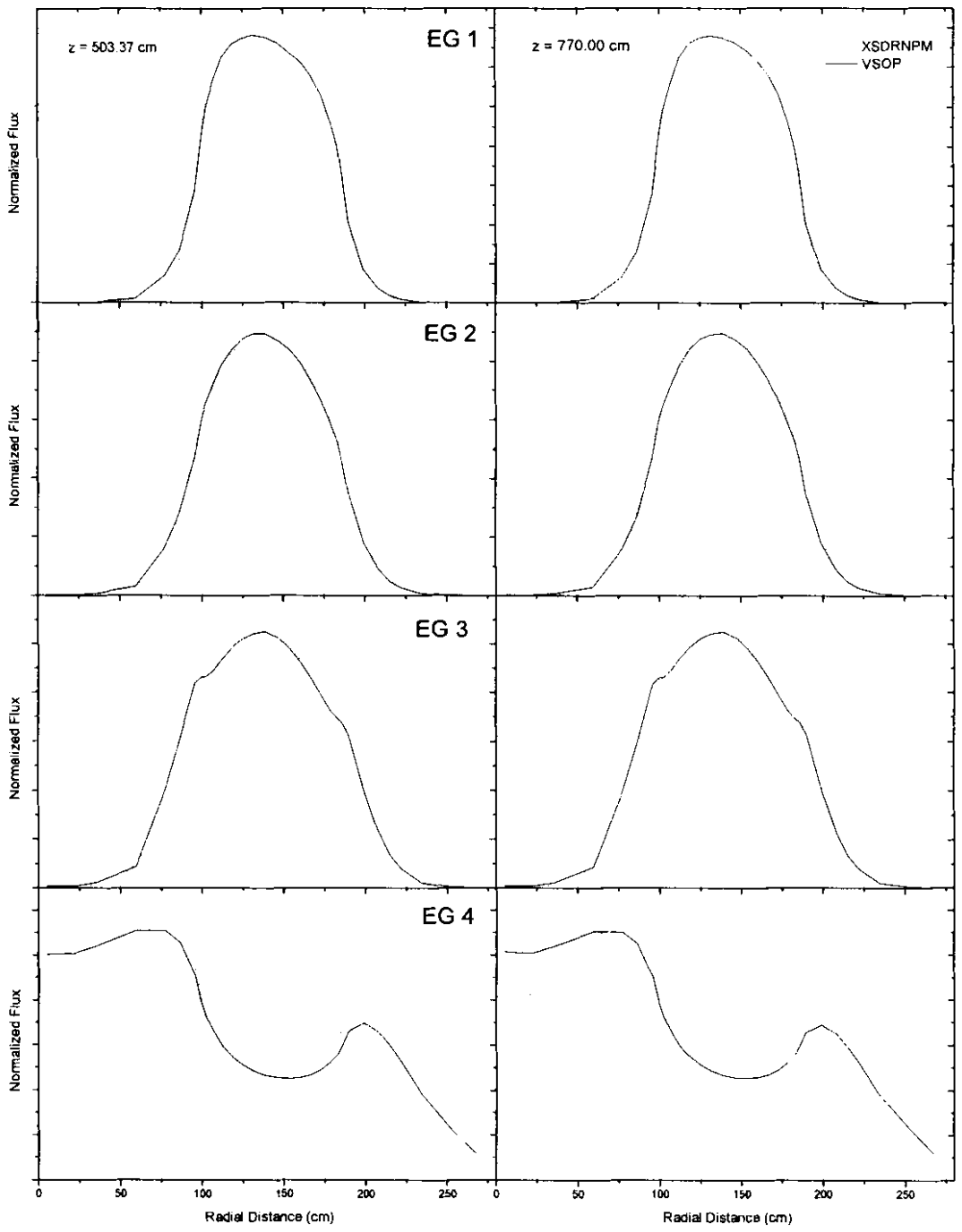

Figure 22: Four Group Radial flux profiles of VSOP and XSDRNPM at Axial Positions 503.37 cm and 770.00 cm

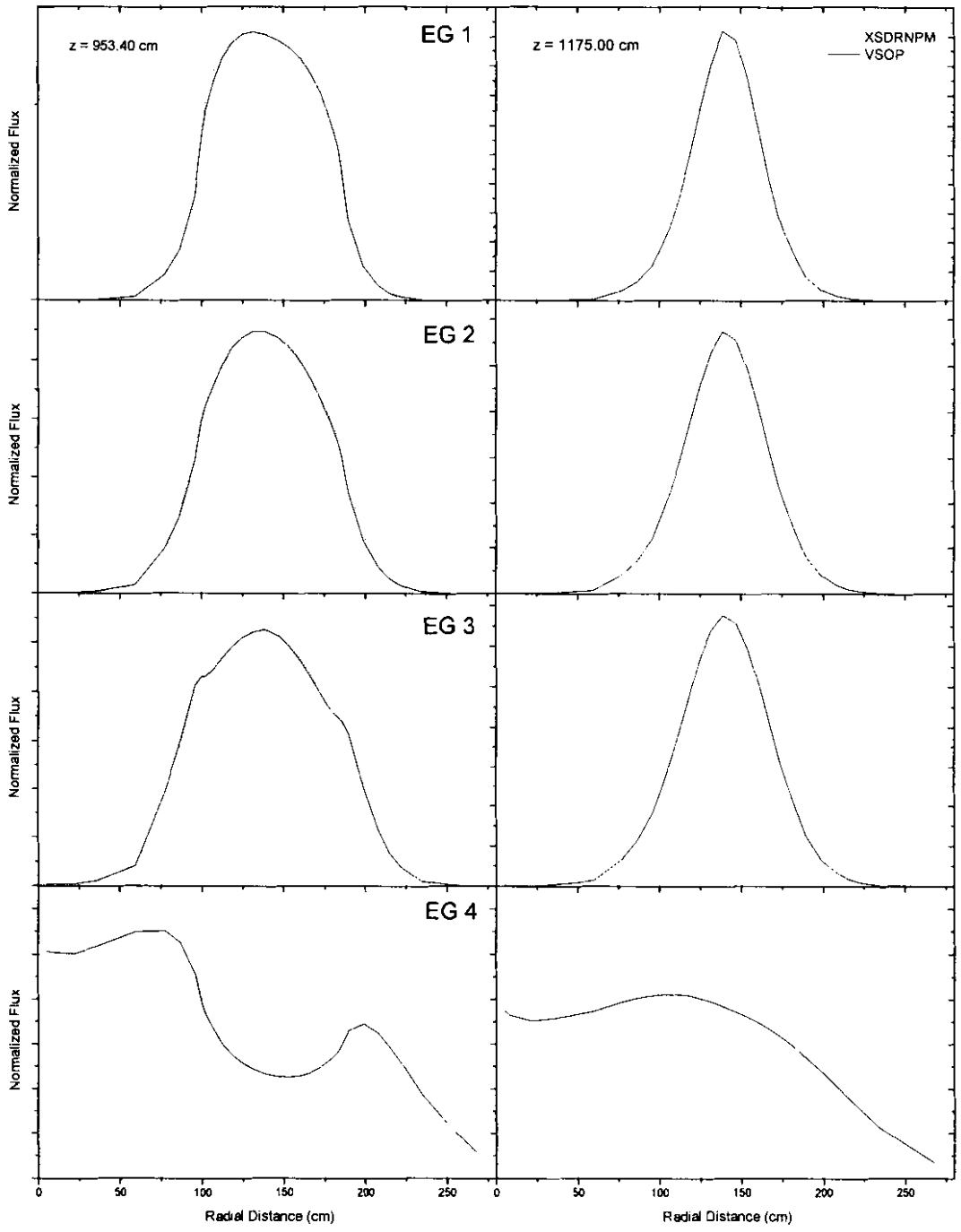

Figure 23: Four Group Radial Flux Profiles of VSOP and XSDRNPM at Axial Positions 953.40 cm and 1175.0 cm

Superimposed on this is the 1-D radial profile as calculated by XSDRNPM. In these figures, the XSDRNPM flux was scaled to that of the VSOP flux by multiplying the XSDRNPM flux by a constant, so that the sum of the least square differences between the two fluxes was a minimum.

The VSOP calculation is done with $\alpha = 0.1141$, and the XSDRNPM results are from case 6, which is the flux calculation with the boundary at x = 275 cm, and with an albedo boundary corresponding to $\alpha = 0.1141$. (See Table 5).
As is expected, in the cases where the two models do not simulate the same geometry, the fluxes vary significantly. This is at the top and the bottom of the core (Figure 21 and Figure 23). In the centre of the core (Figure 22), between $270.03\ cm < z < 953.40\ cm$, the fluxes show better agreement, especially for the three epithermal groups.

The maximum difference that occurs between the two sets of results are shown in Table 19. The differences in the thermal fluxes for the two innermost heights are significant (747.17 cm and 1013.8 cm) while the differences for the uppermost and lowermost positions will obviously be large due to geometry differences.

Table 19: Maximum % Flux Differences between XSDRNPM and VSOP Flux Profiles as a Ratio of the Maximum Flux in Each Energy Group at Different Axial Positions

	Axial position (cm)					
	306.63	513.83	747.17	1013.8	1197.2	1418.8
Energy Group	**Maximum % Difference**					
EG1	17.97	4.39	4.88	5.23	5.33	49.37
EG2	10.37	4.13	4.38	4.54	4.63	32.97
EG3	10.92	5.24	4.75	3.92	3.18	41.71
EG4	53.28	15.21	17.23	18.35	17.86	32.19

The one geometrical difference that is clearly visible is seen at z = 1175.00 cm (Figure 23), which is the position of the cone. Thus the epithermal spectra of VSOP become narrower to correspond with the fuel core width becoming narrower. The VSOP thermal spectrum is also reduced from a double peak to a single peak.

The effect of the control rods inserted into the core is also visible in Figure 21 for z = 62.83 cm. Here the epithermal spectra show the decrease in the right flank of the flux, and the thermal spectrum shows the effect extremely clearly at x ~ 190 cm, where the flux shows a marked dip.

It was also realized that natural boron in the graphite was included in the reactor model using VSOP, whereas it was not included in the XSDRNPM model. To test whether this boron impurity had an effect on the flux profile, VSOP was run with the impurity removed from the model, and the resulting flux profile at the axial position is shown in Figure 24, together with the VSOP case with boron and the XSDRNP flux profile. It can be observed that this neglect of boron in the XSDRNPM model is not the cause for the difference in the flux shape between VSOP and XSDRNPM.

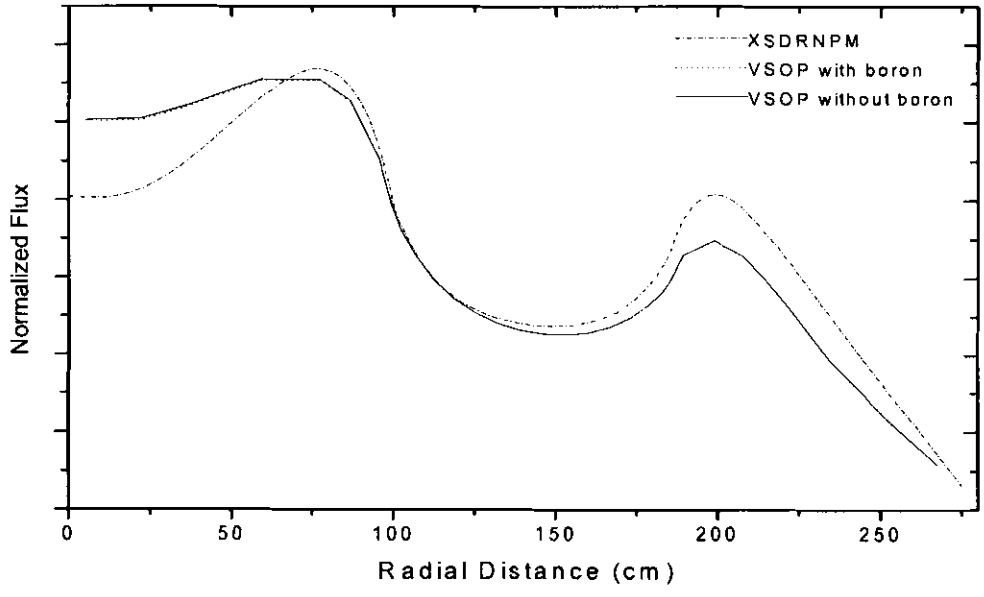

Figure 24: Radial Flux Profile of the Thermal Energy Group of VSOP and XSDRNPM at Axial Position 513.83 cm

A further effect that could give discrepancies is that in VSOP the burnup and thermo-hydraulic effects change axially (i.e., as a function of z because of the layer structure in VSOP), and only those axial regions which match the XSDRNPM burnup will yield the correct set of conditions for the comparison.

In addition, it is recalled that the VSOP calculation is a 2-D, four group, diffusion theory calculation, whereas the XSDRNPM calculation is a 238 group, one dimensional transport theory calculation.

Therefore, it is clear that a lot of effort is required in attempting to understand the differences between the two sets of results. Issues such as differences in cross sections, a one-dimensional model compared to a two-dimensional model and the solution methods (transport compared to diffusion) are only some of these major differences. No further explanations of the differences will be attempted as part of this study.

6.3 The Extrapolation Length

Since the extrapolation length is used to evaluate the vacuum condition, it was felt that it would be worthwhile to calculate its value. The diffusion constant obtained from the output of the VSOP calculation for the thermal energy group is 1.58 cm and the extrapolation length calculated from eq 17 is then

$$\tilde{a} = 3.37\ cm$$

7. CONCLUSION

The first objective in establishing the origin of $\alpha = 0.4692$ has been successfully demonstrated: it is the value when a void is considered beyond the chosen boundary.

With the core barrel and reactor pressure vessel taken into account in defining the boundary condition, the recommended value for α is 0.11414. This was the main objective of the study.

The method used to calculate this value involves calculating the partial currents with the transport theory formulation, which seems to be more robust than using a piecewise numerical formulation at the boundary mesh.

It was also established that the reactivity changed significantly when $\alpha < 0.3$ as compared to $\alpha = 0.4692$. More specifically, the change in reactivity when using $\alpha = 0.11414$ (i.e., with the CB and RPV included) as compared to using $\alpha = 0.4692$ (i.e., the void boundary condition) is 249 pcm. This means that it is necessary to use the correct value.

However, it was found that the leakages from the four energy groups in the VSOP calculations is not heavily dependent on the choice of α. This could mean that the fluences on the components external to the core might not be heavily influenced by the value of α.

A change in reactivity of 208 pcm was found when a single albedo value was used corresponding to $\alpha = 0.11414$, as compared to the case when this constraint effectively did not exist. This is considered to be significant. In addition, the weights to determine α of the four groups of VSOP differed significantly from each other, and the flux shapes at the boundary depended on the type of model (i.e., the material specification at the VSOP boundary) used.

It is noted that the present VSOP software allows only a single value for α. However, given the above observation, it is recommended that four individual alpha values should be implemented corresponding to the four energy groups with values 0.1346, 0.0671, 0.0762 and 0.1885. Ideally the definition of a full albedo boundary condition matrix should be considered, or the position of the boundary condition should be moved further from the core.

The third objective was to look at the sensitivity in reactivity and flux distribution to changes in alpha. Here it was found that the following differences in the model did not change the reactivity and flux shapes significantly:

- defining the region beyond the outer side reflector as homogenous or heterogeneous,
- changing the mesh in XSDRNPM from that of the reference case to match that defined in VSOP,
- defining the core barrel thickness to be 5 cm or 6 cm.

Regarding the fourth objective, it was found that the changes in reactivities when comparing the VSOP calculations against the corresponding XSDRNPM and MCNP calculations compared well.

Regarding the flux profiles, the comparison between the VSOP fluxes and the XSDRNPM fluxes was also good for the three fast energy groups, but not as good for the thermal group.

It is possible that this difference could be resolved using better boundary conditions. However, it should be kept in mind that VSOP as applied in this study is a 2-D diffusion code, whereas XSDRNPM, as applied here, is a 1-D transport code. The angular dependence embedded in XSDRNPM and the spatial 2 dimensional dependence in VSOP will not yield direct comparisons as assumed in this study.

Further work resulting from this study would involve modifying the VSOP software so that more advanced boundary conditions can be specified and

then using this as the first step to resolving the differences in the thermal flux distribution in the VSOP and XSDRNPM results. It should be noted that this difference as it exists presently is not considered to have significant effects on the values of α as presented in this study.

In addition, the MCNP model could be updated to include the RPV in the analysis in order to confirm the reactivity effect seen.

8. BIBLIOGRAPHY

[1] Eskom, http://www.eskom.co.za/education/visit/koeberg/koeberg_bofy.htm

[2] U.S. DOE Nuclear Energy Research Advisory Committee and the Generation IV International Forum, *A Technology Roadmap for Generation IV Nuclear Energy Systems*, December 2002.

[3] Kugeler K, *et.al.*, *Reactor Safety*, Manuscript Textbook, Reactorsicherheit und-technik an der RWTH Aachen, Aachen, 2005

[4] Koster A, *et.al.*, *PBMR design for the future*, Nuclear Engineering and Design 222, pg 231-245, 2003

[5] Kugeler K, *et.al.*, *High Temperature Reactor Technology*, Manuscript Textbook, Reactorsicherheit und-technik an der RWTH Aachen, Aachen, 2005.

[6] Rütten H.J, *et. al.,V.S.O.P.(99/05) Computer Code System*, Jül Report-4189, Forschungszentrum Jülich GmbH, Germany, October 2005

[7] Reitsma F *et.al.*, *An Overview of the FZJ-Tools for HTR Core Design and Reactor Dynamics, the Past, Present and Future*, Mathematics and Computation, Supercomputing, Reactor Physics and Nuclear and Biological Applications, American Nuclear Society, Avignon, France, September 2005.

[8] Naidoo D, *VSOP99 PBMR DP3 V1.0.3 Input Model*, PBMR Internal model, MRI Model number TM 000063, Rev A, Proprietary Class 2, 2005.

[9] Greene N.M. & Petrie L.M., *XSDRNPM: A One Dimensional Discrete Ordinates Code for Transport Analysis*, ORNL-TM-2005/39, ver 5, Vol II, Book 1, Sect. F3, Oak Ridge National Laboratory, Tennessee, 2005.

[10] Duderstadt J.J, Hamilton L.J, *Nuclear Reactor Analysis*, John Wiley and Sons, New York, 1976

[11] Lewis E.E, *et.al.*, *Computational Methods of Neutron Transport*, American Nuclear Society, Inc, Illinois, 1993

[12] Stacey W.M., *Nuclear Reactor Physics*, John Wiley and Sons, NY, 2001

[13] Fowler T.B., *et.al.*, *Nuclear Reactor Core Analysis Code: CITATION*, ORNL-TM-2496, Rev. 2, Oak Ridge National Laboratory, Tennessee, October 1971

[14] Case K M, Zweifel P F, *Linear Transport Theory*, Addison-Wesley, Massachusetts, 1967

[15] X-5 Monte Carlo Team, *MCNP- A General Monte Carlo N-Particle Transport Code*, LA-UR-03-1987, Ver 5, Los Alomos National Laboratory, California, 1987

[16] Reitsma F, *The Pebble Bed Modular Reactor Layout and Neutronic Design of the Equilibrium Cycle, PHYSOR 2004 – The Physics of Fuel Cycles and Advanced Nuclear Systems*, American Nuclear Society, Chicago, April 2004.

[17] van Heerden G, *TINTE PBMR 400DP3 Model*, PBMR Internal Report, MRI Model No TM000010, Rev 1, Propriety Class 2, 2005.

[18] Gerwin H, *The Two Dimensional Reactor Dynamic Programme Tinte*, Jülich - 2167, Nuclear Research Facility Jülich, Jülich, 1987

[19] Rütten H J, Haas K A, *VSOP. (99/3) – Update 2, PBMR- Version*, Jül-2897, Forshungszentrum Julich, July 2004.

[20] Hamrin D.R., *SCALE: A Modular Code System for Performing Standardized Computer Analyses for Licensing Evaluation*, ORNL-TM-2005/39, Oak Ridge National Laboratory, Tennessee, April 2005

[21] Jing X, *et.al.*, *Predictions calculations and experiments for the first criticality of the 10 MW High Temperture Gas cooled reactor test module*, Nuclear Engineering and Design, 218 , pg 43 – 49, 2002.

[22] Reitsma F, *PBMR Core Neutronics 400 MW Design*, PBMR Internal Report, Report No 13905, Rev 3c, Centurion, August 2005

[23] Naidoo D, *VSOP Input Model PBMR400 DP3: VSOP Material Specifications*, PBMR Internal Report, Report No T000076, Rev A, Centurion, September 2004

[24] Naidoo D, *VSOP Input Model PBMR400 DP3: Geometrical Description*, PBMR Internal Report, Report No 025320, Rev 1, Centurion, 2005

[25] Naidoo D, *VSOP Input Model PBMR400 DP3: Thermix Description*, PBMR Internal Report, Report No 026102, Rev 1, Centurion, 2005

[26] Stoker C, *Origen S Fuel Depletion Input Model,* PBMR Internal Model, MRI Model number TM000050, Rev A, Proprietary Class 2, Centurion 2005.

[27] Stoker C, *PBMR 400 MW 6 Pass ORIGEN-S Model*, PBMR internal report, Report No T000142, Rev1, Centurion, 2006.

[28] Stoker C & Reitsma F, *PBMR Fuel Sphere Source Terms*, 2nd International Topical Meeting on High Temperature Reactor Technology, Beijing, September, 2004

[29] Albornoz F, *MCNP, Core and Core Structures Model Report*, PBMR Internal Report, Report No. 015684, Rev 1, Centurion, April 2006

9. APPENDICES

9.1 Appendix A: Input Data File XSDRNPM

The input file for case 2 is listed here.

```
=XSDRNPM
REACTOR CORE - CORE AVERAGE TO SINGLE ORIGEN LIB
-1$$  5000000
0$$   A3 34 A5 37 E
1$$   2 13 205 1 0 9 86  8 3 1 200 200 0 0 0
2$$  -1 1 1 0 A7 0  E
3$$   1 E
4$$   0 4 0 -1 0 0 E
5**   1.0E-05 1.0E-05 1.0  E    T
13$$      78R1 2 3 4 5 6 7 8 9
14$$    111      999
      90232    91233    92233    92234    92235    92236    92237
      92238    93237    93238    94238    94239    94240    94241
      94242    94242    95241    95601    95242    95243    96242
      96243    96244    54135    54136    36083    40095    42095
      42097    43099    44101    44103    45103    45105    46105
      46108    47109    48113    53131    54131    54133    55133
      55134    59141    59143    60143    60144    60145    60146
      61147    61148    61601    62147    62148    61149    62149
      62150    61151    62151    62152    63153    63154    63155
      64155    64156    64157     8016    38090    39090    39091
      41095    55137    56140    57140    58143     6012
                       555  666  777  888  789    555   666  777
15**  1.0 77R1.0E-20   1.0  1.0  1.0  1.0  1.00  0.918 0.941 0.881
   T
33##  F1.0    T
35** 2I0 18I10 26I46 4I93 8I100 22I109 12I135 22I150 8I176 4I185
     12I192 24I215 8I261 3I275 2I287.50 6I293.5 7I310.0  328
36$$   3R1  19R2  27R3  5R4   9R5   23R5   13R5   23R5   9R5   5R6
      13R7  25R8   9R9  4R10  3R11   7R12   8R13
39$$    5   2   7   2    1    3    8    9    4    5   6   5   6
40$$  13R3
51$$  44R1 72R2 45R3 77R4
 T
END
```

9.2 Appendix B: File Connection Data

VSOP was run with a batch file using a DOS prompt under Windows.
Each command in the batch required references to input and output files, and these references were contained in .fil files, which are listed here.

P400-s.fil

```
  5 p400-s.i                                SFOI
  6 p400-s.o                                SFUO
 15 p400-s.rst                              SUUB
 16 ..\libraries\gam                        SFOI
 18 ..\libraries\therm1515                  SFOI
 30 ..\libraries\p400dp3v103_resint         DUOI   292
 35 p400dp3v103_rstcit                      SUUB
 37 p400dp3v103_geom                        SFUB
 42 p400dp3v103_macsig                      SFUB
 63 ..\libraries\adage                      SFOI
 97 p400-s.keff                             SFUB
ENDFCD
```

P400-e.fil

```
  5 p400-t.i                                SFOI
  6 p400-t.o                                SFUO
 14 p400-e.rst                              SUOI
 15 p400-t.rst                              SUUB
 16 ..\Libraries\gam                        SFOI
 18 ..\libraries\therm1515                  SFOI
 30 ..\libraries\P400DP3V103_resint         DUOI   292
 35 p400dp3v103_rstcit                      SUUB
 37 p400DP3V103_geom                        SFUB
 42 p400DP3V103_macsig                      SFUB
 59 p400dp3v103_tempstat                    SFOB
 63 ..\libraries\adage                      SFOI
 68 p400-t.phiform                          SFUB
 80 p400-t.powform                          SFUB
 94 p400dp3v103_heat                        SFOI
 95 p400dp3v103_edn                         SFOI
 96 p400-t.temp                             SFUB
 97 p400-t.keff                             SFUB
ENDFCD
```

P400-t.fil

```
  5 p400-t.i                                SFOI
  6 p400-t.o                                SFUO
 14 p400-e.rst                              SUOI
 15 p400-t.rst                              SUUB
 16 ..\Libraries\gam                        SFOI
 18 ..\libraries\therm1515                  SFOI
 30 ..\libraries\P400DP3V103_resint         DUOI  292
 35 p400dp3v103_rstcit                      SUUB
 37 p400DP3V103_geom                        SFUB
 42 p400DP3V103_macsig                      SFUB
 59 p400dp3v103_tempstat                    SFOB
 63 ..\libraries\adage                      SFOI
 68 p400-t.phiform                          SFUB
 80 p400-t.powform                          SFUB
 94 p400dp3v103_heat                        SFOI
 95 p400dp3v103_edn                         SFOI
 96 p400-t.temp                             SFUB
 97 p400-t.keff                             SFUB
ENDFCD
```

P400-t2.fil

```
  5 p400-t.i                                SFOI
  6 p400-t2.o                               SFUO
 14 p400-t.rst                              SUOI
 15 p400-t2.rst                             SUUB
 16 ..\Libraries\gam                        SFOI
 18 ..\libraries\therm1515                  SFOI
 30 ..\libraries\P400DP3V103_resint         DUOI  292
 35 p400dp3v103_rstcit                      SUUB
 37 p400DP3V103_geom                        SFUB
 42 p400DP3V103_macsig                      SFUB
 59 p400dp3v103_tempstat                    SFOB
 63 ..\libraries\adage                      SFOI
 68 p400-t2.phiform                         SFUB
 80 p400-t2.powform                         SFUB
 94 p400dp3v103_heat                        SFOI
 95 p400dp3v103_edn                         SFOI
 96 p400-t2.temp                            SFUB
 97 p400-t2.keff                            SFUB
ENDFCD
```

P400-t3.fil

```
  5 p400-t.i                                SFOI
  6 p400-t3.o                               SFUO
 14 p400-t2.rst                             SUOI
 15 p400-t3.rst                             SUUB
 16 ..\Libraries\gam                        SFOI
 18 ..\libraries\therm1515                  SFOI
 30 ..\libraries\P400DP3V103_resint         DUOI   292
 35 p400dp3v103_rstcit                      SUUB
 37 p400DP3V103_geom                        SFUB
 42 p400DP3V103_macsig                      SFUB
 59 p400dp3v103_tempstat                    SFOB
 63 ..\libraries\adage                      SFOI
 68 p400-t3.phiform                         SFUB
 80 p400-t3.powform                         SFUB
 94 p400dp3v103_heat                        SFOI
 95 p400dp3v103_edn                         SFOI
 96 p400-t3.temp                            SFUB
 97 p400-t3.keff                            SFUB
ENDFCD
```

P400-ee.fil

```
  5 p400-ee.i                               SFOI
  6 p400-ee.o                               SFUO
 14 p400-t3.rst                             SUOI
 15 p400-ee.rst                             SUUB
 16 ..\libraries\gam                        SFOI
 18 ..\libraries\therm1515                  SFOI
 30 ..\libraries\P400DP3V103_resint         DUOI   292
 35 p400dp3v103_rstcit                      SUUB
 37 p400DP3V103_geom                        SFUB
 42 p400DP3V103_macsig                      SFUB
 59 p400dp3v103_tempstat                    SFOB
 63 ..\libraries\adage                      SFOI
 68 p400-ee.phiform                         SFUB
 80 p400-ee.powform                         SFUB
 96 p400-ee.temp                            SFUB
 97 p400-ee.keff                            SFUB
ENDFCD
```

9.3 Appendix C: XSDRNPM Extraction File AUG07_06

Relevant data from the output file from XSDRNPM was extracted using the program aug07_06. Using eq 38 and eq 39, the 238 x 2 partial currents were calculated. These partial currents were compressed into 4 x 2 partial currents using eq 43. Eq 37 was then used to determine the 4 α values, and using the weights, the single α value was calculated using eq 44. The complete source code is listed below.

```
      program aug07_06
      character *72 file1,file2
      real r(1000),alpha(4),wts(4)
      real jneg(4,1000), jpos(4,1000)

      open(20,file='aug07-06.txt')
      write(20,2007)

2007  format(' fortran file: aug07-06.f90'/' uses jneg and jpos'/)
      file1 = 'c:\vvn\alpha\alpha60\pbmr-a-60.out'
      file2 = 'c:\vvn\alpha\alpha70\pbmr-a-70.out'
      call one(r,jneg,jpos,npts,file1)

      call two(r,jneg,jpos,npts,alpha,rval)
      write(20,2001)
      write(20,2000) rval,(alpha(i),i=1,4)

      call three(wts,file2)
      write(20,2030)
      write(20,2020) (wts(i),i=1,4)

      call four(alpha, wts, a)
      write(20,*)
      write(20, 2040) a

2040  format(' the weighted alpha value is: ',f10.5)
2020  format(4(1x,f12.5))
2030  format(' Weights from importances')
2000  format(f10.2,2x,4(2x,f10.4))
2001  format(' position and alpha values according to 4 eg')
      end
!*******************************************************
      subroutine four(alpha, wts, a)
      real alpha(4), wts(4),a

!           evaluate the weighted value of alpha

      a = 0.0
```

```
      do i = 1,4
            a = a + wts(i)*alpha(i)
      end do

      return
      end

!*********************************************************
      subroutine three(wts,file2)
      character *72 file2
      character *20 text1,text2
      real wts(4),rwts(4)
      open(5,file=file2)
!     read in the weights from the adjoint flux solution
      text1 = 'cell averaged fluxes'
      do
            read(5,1000) text2
            if(text1.eq.text2) exit
            end do

            do i = 1,11
                  read(5,1000) text2
            end do

            read(5,1010) rwts(4),rwts(3),rwts(2),rwts(1)
            rsum = 0.0

            do i = 1,4
                  rsum = rsum + rwts(i)
            end do

            do i = 1,4
                  wts(i) = rwts(i)/rsum
      end do

1010  format(6x,4(es12.5,1x))
1000  format(a20)
      close(5)
      return
      end

!*********************************************************
      subroutine two(r,jneg,jpos,npts,alpha,rval)
      real r(1000),alpha(4)
      real jneg(4,1000), jpos(4,1000)
      real c(4)

!     evalutes the value of alpha according to the jmin/jpos calc
      i = 0
      do
            i = i + 1
            if(r(i).gt.275.0) exit
            end do
            ip = i - 1
            rval = r(ip)
            do i = 1,4
            c(i) = jneg(i,ip)/jpos(i,ip)
            alpha(i) = 0.5*(1.-c(i))/(1.+c(i))
            end do

            open(29,file='current')
            do i=1,4
```

```
                write(29,2005) i,jneg(i,ip),jpos(i,ip)
            end do

2005    format(i5,2x,es12.4,2x,es12.4)
        return
        end

!*********************************************************
        subroutine one(r,jneg,jpos,npts,file1)
        character *72 file1,file2
        character *12 text1,text2
        character *15 text5,text6
        character *20 text3,text4
        character *34 text7,text8
        real wts(24),cosu(24),r(1000),aphi(8)
        real jneg(4,1000), jpos(4,1000)
        integer jstart(4), jstop(4)

! this programs reads in the angular fluxes, and calculates the partial
! currents in the four energy groups of the current model of VSOP
        open(5,file=file1)
!_______________
            text1 = '   35* array'

            do
            read(5,1000) text2
            if(text2.eq.text1) exit
            end do

            backspace(5)
            read(5,1001) npts
!_______________
            text3 = 'quadrature constants'

            do
            read(5,1002) text4
            if(text3.eq.text4) exit
            end do

            read(5,1002) text4
            do i = 1,24
            read(5,1003) wts(i),cosu(i)
            end do
!_______________
            text5 = '  int     radii'
            do
            read(5,1004) text6
            if(text5.eq.text6) exit
            end do
            do i = 1,npts
            read(5,1005) r(i)
            end do
!_______________
!           open(8,file='scratch.out',action = 'READWRITE')
            text7 = ' flux by angle and point for group'
            do
            read(5,1006) text8
            if(text7.eq.text8) exit
            end do
            backspace(5)
            jstart(1) = 1
            jstart(2) = 45
```

```
              jstart(3) = 117
              jstart(4) = 162
              jstop(1) = 44
              jstop(2) = 116
              jstop(3) = 161
              jstop(4) = 238
!   energy groups
do i = 1,4
   do k1=1,npts
        jneg(i,k1) = 0.0
        jpos(i,k1) = 0.0
   end do
   do j = jstart(i), jstop(i)
       read(5,1006) text8   ! flux by angle
       do k = 1,3
              k3 = 8*(k-1)
              read(5,1006) text8         ! blank line
              read(5,1006) text8         ! col header
              do k1 = 1,npts
              read(5,1010) (aphi(k2),k2=1,8)
              do k2 = 1,8
              if(cosu(k2+k3).lt.0.0) then
                jneg(i,k1) = jneg(i,k1) +
abs(cosu(k2+k3))*wts(k2+k3)*aphi(k2)
              else
                jpos(i,k1) = jpos(i,k1) +
abs(cosu(k2+k3))*wts(k2+k3)*aphi(k2)
              end if
              end do
               end do
       end do
    end do
end do
close(5)
!  **********************************
1010   format(5x,8(1x,e12.0))
1011   format(f10.4,2x,es12.4)
1007   format('EG',i1)
1008   format('EG',i2)
1009   format('EG',i3)
1006   format(1x,a34)
1000   format(a12)
1001   format(15x,i4)
1002   format(71x,a20)
1003   format(58x,e12.0,1x,e12.5)
1004   format(1x,a15)
1005   format(6x,e12.0)
              return
              end
```